Topics on the information theoretic limits of quantum information processing and its implementation

by

Sadegh Raeisi

A thesis
presented to the University of Waterloo
in fulfilment of the
thesis requirement for the degree of
Doctor of Philosophy
in
Physics-Quantum Information

Waterloo, Ontario, Canada, 2014

Author's Declaration

I hereby declare that I am the sole author of this thesis. This is a true copy of the thesis, including any required final revisions, as accepted by my examiners.

I understand that my thesis may be made electronically available to the public.

Abstract

Recent advances in quantum technologies enabled us to make "large" quantum states and pushed towards examining quantum theory at the macroscopic level. However observation of quantum effects at a macroscopic level still remains a demanding task. In this thesis we try to address one of the challenges and propose and explore some new solutions.

One of the obstacles for observation of macroscopic quantum effects is the sensitivity to the measurement resolution. For many different cases, it has been observed that the precision requirement for measuring quantum effects increases with the system size. We formalize this as a conjecture that for observation of macroscopic quantum effects, either the outcome precision or the control precision of the measurements has to increase with system size. This indicates that the complexity of macroscopic quantum measurement increases with the system size and sheds some lights on the quantum-to-classical transition at the macroscopic level.

We also introduce a technique to go around the sensitivity problem for observation of micro-macro entanglement. We propose that using a unitary deamplification process, one can bring the system back to the microscopic level where the measurements are less demanding and quantum effects are easier to verify. As the unitary processes do not change the entanglement, this serves as a verification tool for micro-macro entanglement.

We also explored the connection between quantum effects and thermodynamics of macroscopic quantum systems for two specific cases. For one, we investigated the effect of entanglement in composite bosons and Bose-Einstein condensation. We showed that as the state of the composite boson approaches a maximally entangled state, the condensation rate also approaches one.

The other case we considered was heat-bath algorithmic cooling. We proved the cooling limit of this class of thermodynamic transformations and showed that it decreases exponentially with the number of qubits.

We also developed an entropic version of Mermin's inequality. Here the idea is to develop a tool to reveal the entanglement in many-body quantum systems based on the entropy of the measurement outcomes. We introduce a new inequality that holds for locally realistic models, yet can be violated with quantum measurements. One of the nice features of this inequality is that it can be violated maximally with quantum measurements. This resembles the GHZ paradox but for entropies of the measurement outcomes.

Acknowledgements

This is one of those places that I get to thank those people who have contributed to my long journey up to this point. It is a challenge to remember everyone and to find a place to start, among all the people that I owe my gratitude. I start with my family who have been by my side all these years. I cannot even begin to thank them, especially my mother who has always believed in me, especially my dad, who, in his own way, has always had my back, and my little sister who has always inspired me.

Next is my supervisor, Dr. Michele Mosca. I cannot possibly thank him enough. I have learned a great deal from him through these years that he has supervised me and he has played a significant role in the kind of physicist that I am going to be. Also he has supported me when it wasn't easy to support me and had my back. I am really grateful for all of his support.

I should also thank my committee members, Dr. Resch, Dr. Mariantoni and Dr. Emerson and my external examiner, Prof. Vedral, for their scientific support and guidance.

Last but not least are my friends whose presence made my tough days tolerable. I am really thankful, Guys!

Dedication

I would like to dedicate my thesis to my Mom, to my Dad and to my little sister who have had my back all these years.

Table of Contents

List of Figures

x

Chapter 1

Introduction

Quantum theory has been investigated at different scales and it is well accepted for microscopic systems. Predictions and phenomena such as entanglement and non-locality has been examined with different techniques and it seems that quantum theory gives a good description of these phenomena.

Recent progress in the control and the measurement of quantum systems provided the opportunity to push towards testing quantum mechanics over "larger" systems. [67, 107, 10]. Yet it is a challenge to reconcile the macroscopic world that we experience in our everyday life with quantum theory. Specifically, it is unclear when and how systems stop behaving according to quantum theory and become classical.

Microscopic versus macroscopic in quantum mechanics can be studied at two different levels: state preparation and measurement. For state preparation, a wide variety of quantum states like Bell states are microscopic whereas, states like GHZ state and NOON state are often recognized macroscopic. Note that in general the border between micro and macro is not clear, there are different definitions for macroscopic states which categorises states differently. Similarly quantum measurements could be microscopic and macroscopic. Microscopic measurements usually deal with a few particles or quantum degrees of freedom whereas macroscopic measurements can measure states that involves "large" number of particles and belong to large Hilbert spaces.

From this point of view, four different setting can be perceived, which involves the two possible kind of measurements on the two possibilities for the state. See figure (1.1).

Probably the most exciting category is the one where a macroscopic measurement is applied on a macroscopic state. This is closely connected to studies on quantum-to-classical transition. Our conjecture on the effect of coarse-graining falls into this category.
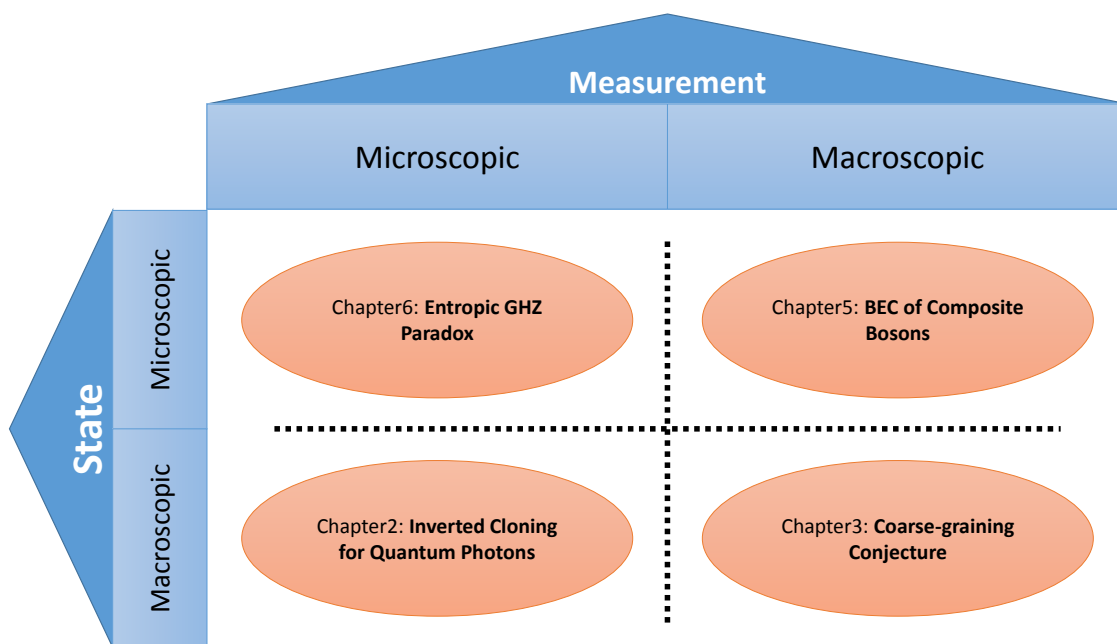
Figure 1.1: An overview of how each chapter of this thesis fits into the big picture of understanding quantum mechanics at microscopic and macroscopic level. Both measurement and the state preparation in quantum mechanics could be both microscopic and macroscopic and this gives four different possibilities for quantum measurements.

One of the approaches to understand the quantum-to-classical transition inside quantum theory is through the imperfections of measurements, where the classical theory is explained as an extreme of the quantum theory where measurements are coarse-grained [118, 132, 94]. For many quantum systems the required measurement or control precisions for observing macroscopic quantum effects increases with the system size [118, 132, 94, 139, 180, 70]. and as a result, it gets almost impossible to observe the quantum effects at a macroscopic level. For instance, observation of an optical Schrödinger's cat was claimed in [47], but later it was shown that even without any decoherence in the experiment, it still would be impossible to verify the claim with the experimental data because of the coarse-graining in the photon detections. More specifically, ref. [139] showed that even with a small coarse-graining, it would be possible to reconstruct the outcomes with classical correlations instead of entanglement. They also suggested that this may be a general property for macroscopic quantum systems. There was however a counterexample [87] where a robust measurement for the observation of macroscopic states of photons was proposed. We showed that even in the case of the corresponding counterexample, high precision is still a requirement, but it shows up differently, specifically as the control precision for the measurement. We also formalized a conjecture that for observation of macroscopic quantum effects, either the outcome precision or the control precision of the measurements has to increase with the system size[180]. This work makes up chapter (3) of this thesis, most of which is published in [180].

Although observation of quantum effects like micro-macro entanglement at a macroscopic level turned out to be challenging, we proposed a technique for their verification. The idea is to transform the macro-macro state to a micro-micro state through a unitary transformation which does not change the entanglement. So if we detect any entanglement for the micro-micro state, it implies the existence of the entanglement at the macroscopic level as well. Note that this falls under the category of microscopic measurements on a macroscopic state. This work makes up chapter (2) of this thesis, most of which is taken from the published paper in [140]. Our idea has been modified and adapted to other implementation techniques of micro-macro state [69, 160, 68]. It also has been used in [114, 25] for the first optical realization of Schrödinger's cat.

The other category is to find a macroscopic measurement that could illustrate quantum effects like entanglement at a microscopic level. For instance, it is shown that some thermodynamic properties like magnetic susceptibility [182] and heat capacity[183] can be used to witnesses entanglement. Chapter (5) of this thesis attempts to achieve a similar goal. More specifically, we investigated the Bose-Einstein condensation in a system of composite particles and the effect of the entanglement between the entities of the composite bosons. Specifically, we considered bi-bosons and bi-fermions and showed that as the entanglement

inside the composite boson increases, the condensation rate approaches one. This work was done in collaboration with D. Kaszlikowski's group. The results of this work are presented in chapter (5) most of which also appears as a preprint on the arxiv [108].

The final chapter falls into the well-studied category of microscopic measurements on microscopic states. One of the famous examples in this category is the Bell inequality which is often used as a witness of entanglement [12]. Later it was generalized to multi-partite systems by Mermin [119]. In parallel there has been some attempts to establish violations of local realism in terms of information rather than correlation. This may be motivated by two points, first, information may be more fundamental than correlation [20, 84, 30] and second, it may be easier to understand the transition from microscopic regime to the macroscopic regime in terms of the information. Here we use the "triangle principle" method introduced in [100] and extended it to construct Bell-type inequalities for multi-partite systems. We introduce a new entropic distance and use it to construct an inequality similar to Mermin's inequality. Interestingly, this inequality can be violated maximally with quantum measurements. This is similar to the GHZ paradox, however it works with the entropy of the measurement outcomes instead of the outcomes directly. This part is presented in chapter (6). Most of the material also appeared in a preprint on arxiv [137].

We also looked at another example related to quantum thermodynamics, namely heat-bath algorithmic cooling techniques which does not really fall under any of the categories. We showed that the work extraction limit in this class of transformations improves exponentially with the number of particles involved in the cooling process. Although this example is not as directly connected to the main context, it provides valuable insights to a problem that has been open for almost 10 years, namely, we proved the cooling limit of all the heat-bath algorithmic cooling techniques. The result of this work is presented in chapter (4), most of which is taken from [138].

The structure of this thesis is as follows. In the second chapter, the idea of inverted cloning for verification of micro-macro entanglement is presented. Most of the text is taken from the published work in [140]. The third chapter focuses on our conjecture that high precision is required for the observation of macroscopic quantum effects. Most of the text of this chapter is taken from the published paper [180]. In chapter (4), we explain the details of our result on heat-bath algorithmic cooling. The content of this chapter is also published as a preprint on arxiv [138]. Chapter (5) presents our results on the Bose-Einstein condensation of composite bosons. The content of this chapter is also on arxiv[108]. The last chapter presents our entropic version of the GHZ paradox and the details of the derivation. The content can also be found in [137]. In each chapter I also explain my contribution in the corresponding project.

Chapter 2

Inverted Cloning for Quantum Photons

Most of the content of this chapter was published in [140]. I proposed the main idea of the paper and did some of the calculations, and double checked the rest of them. I also contributed in writing the paper.

2.1 Introduction

2.1.1 State Cloning in Quantum Mechanics

The no-cloning theorem [184, 48] states that it is impossible to build a quantum copying machine that would perfectly copy arbitrary quantum states. This is a direct consequence of the linearity of time evolution in quantum physics. It is also essential in order to rule out the possibility of superluminal communication using quantum entanglement [81]. However, approximate quantum cloning is possible [28] and has been studied extensively. Different types of quantum cloners have been introduced, including universal cloners [28, 72], which clone all input states equally well, and phase-covariant cloners [26], which produce equally good copies for all input states that lie on the equator of the Bloch sphere.

In all cases, the fidelity of the clones has to satisfy certain bounds, whose exact form depends on the type of cloner considered. One way of understanding these bounds is to realize that the clones cannot contain more information about the initial state than the initial state itself [27]. One may then wonder if the clones contain exactly the same amount of information as the initial state (or less). In the case of optimal phase-covariant cloning it is easy to see that the answer is yes because the cloning transformation can be realized in

5

a unitary fashion. It is thus in principle possible to invert the cloning transformation and recover the initial state. The answer can be shown to be yes for universal cloning as well, but one has to use more sophisticated arguments based on state estimation, as the cloner uses auxiliary systems and is thus non-unitary if only inputs and clones are considered [27].

Implementations of quantum cloning have been studied extensively over the last decade [152]. A particularly simple and intuitive way of realizing quantum cloners in the context of quantum optics (where the inputs are photons) is by using stimulated emission; in this case the bounds on the fidelity of the clones can be seen as being due to the unavoidable presence of spontaneous emission [165, 45]. Both universal [104] and phase-covariant [126] quantum cloners have been realized based on stimulated parametric down-conversion. However, inverting these cloning transformations has not been considered so far. The feasibility of this inversion is the topic of the present paper. Focusing on the case of phase-covariant cloning, we take into account the most important experimental imperfection, namely photon loss.

2.1.2 Quantum Optics Background

Here we introduce some basic background of quantum optics that we used in this work. We start by the description of the quantum state. We use the polarization degree of freedom of the photons. In particular, the initial state that we use in our proposal is an entangled photon pair in a polarization singlet state

$$|\psi_-\rangle = \frac{1}{\sqrt{2}}(a_h^\dagger b_v^\dagger - a_v^\dagger b_h^\dagger)|\Omega\rangle, \tag{2.1}$$

where h and v denote horizontal and vertical polarization and $|\Omega\rangle$ is the vacuum state for all modes.

The other element that we use is the parametric down conversion process which is given by the following Hamiltonian

$$H = i\chi a_h^\dagger a_v^\dagger + h.c.. \tag{2.2}$$

This corresponds to type-II collinear parametric down-conversion [126, 47]. The coupling constant χ includes the non-linear coefficient of the crystal and the amplitude of the pump laser. The spatio-temporal mode a in the Hamiltonian has to be indistinguishable from that of the input photon in order for stimulated emission to occur [165, 45]. We use this process as the phase-covariant cloner.

We also consider the photon loss in our proposal. For this purpose, we use the typical beam-splitter model for the loss. Specifically, we model a channel with transmitivity η, with a beam-splitter with transmission rate $\sqrt{\eta}$.

2.1.3 Micro-Macro Entanglement

Experimentally inverting quantum cloning would be a striking demonstration of the information preservation in the cloning process. We will in particular focus on the case where the initial input photon is entangled with another photon. The preservation of this entanglement after the cloning process and its inversion is a good criterion for verifying if the original photon is indeed regenerated with its quantum character intact. However, there is another reason why this scenario is particularly interesting. There is a recent experiment [47] where one photon from an entangled pair was phase-covariantly cloned, and where the number of clones produced was up to tens of thousands. The authors of [47] claimed to have demonstrated micro-macro entanglement between one original photon and a large number of photons (the clones). This claim was subsequently challenged [157], leading to a number of detailed theoretical investigations [161, 168, 167, 139]. The conclusion of this debate is that it is not easy to prove the existence of micro-macro entanglement in this system experimentally without too many assumptions. The present approach via the inversion of the cloning transformation is one possible avenue. If there is still entanglement after cloning and inverted cloning, then there definitely had to be micro-macro entanglement after the cloning step. Our proposal with some modification has been exploited recently for experimental demonstration of micro-macro entanglement [114, 25].

2.2 Proposal for Inverted Cloning

We now describe the system that we are considering in more detail; see also Figure 1 for the setup. The initial photon pair is in the polarization singlet state in Eq. (2.1). The photon in spatial mode B is detected directly in a polarization-sensitive way and serves as a herald. The photon in spatial mode A is subjected to the unitary phase-covariant cloning transformation $U = e^{-iHt}$, where the Hamiltonian is the spontaneous parametric down-conversion (SPDC) Hamiltonian in Eq. (2.2) which is

$$H = i\chi a_h^\dagger a_v^\dagger + h.c.. \tag{2.3}$$

Identifying h and v with the north and south poles of the Bloch sphere and introducing equatorial modes $a_\phi = \frac{1}{\sqrt{2}}(e^{i\frac{\phi}{2}}a_h + e^{-i\frac{\phi}{2}}a_v)$ and $a_{\phi\perp} = a_{\phi+\pi}$, one has

$$H = \frac{i\chi}{2}(a_\phi^{\dagger 2} + a_{\phi\perp}^{\dagger 2}) + h.c.. \tag{2.4}$$

The Hamiltonian thus corresponds to a sum of two squeezers for any two orthogonal equatorial modes. As a consequence, U factorizes into two independent unitaries, one for a_ϕ

7
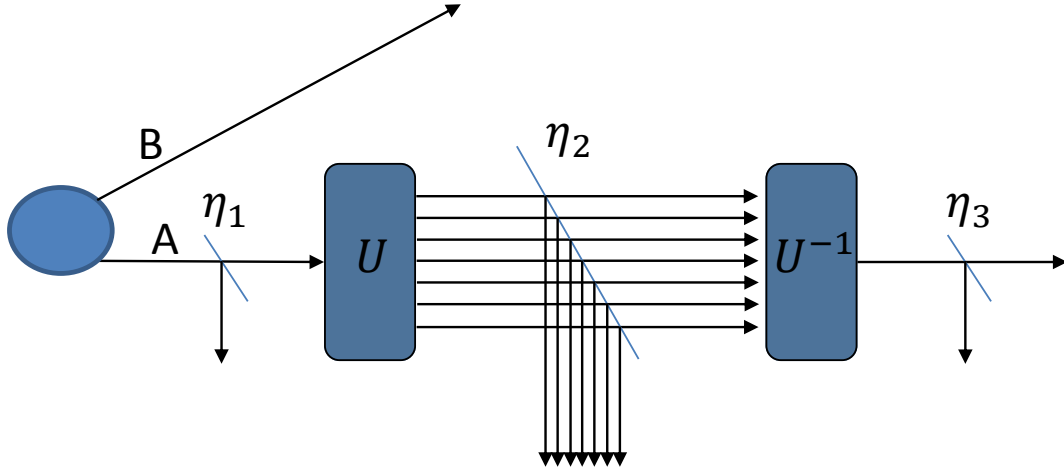
Figure 2.1: Setup considered in this paper. A source creates a pair of entangled photons. The photon in mode B is detected directly. The photon in mode A is cloned by the phase-covariant cloning transformation U, then this transformation is inverted, U^{-1}. The pump laser beams necessary for implementing the cloning transformations are not shown. Losses before, in between and after the cloning transformations are taken into account through the transmission factors η_1, η_2 and η_3. We are interested in the regime where the final state in mode A is again at the single-photon level. We study whether the final state of modes A and B can be shown to be entangled using the witness W of Eq. (4), which is based on polarization-sensitive photon counting in both modes. The presence of (strong) entanglement between A and B in the final state can be interpreted as showing that the quantum information present in the original photon in mode A is regenerated in the final single-photon level state of mode A. Furthermore, any entanglement that is detected between A and B in the final state implies that the multi-photon state created by the first cloning transformation in A was entangled with the single photon in mode B (micro-macro entanglement), since entanglement cannot be created locally.

and one for $a_{\phi\perp}$. Note that since the choice of ϕ is arbitrary, we will use the notation a and $a_\perp$ for the equatorial modes for simplicity.

The inverted cloning transformation U^{-1} can be implemented by changing the sign of χ. Physically this can be done by changing the phase of the pump beam for the down-conversion process. Note that if U^{-1} acted on a single-photon input state, it would create a large number of clones in full analogy with U, with changes only in certain phase factors that depend on the sign of χ. However, acting after U it has the effect of converting a multi-photon state back to the single-photon level.

We want to study the entanglement in the final state, i.e. after cloning and inverted cloning. In the absence of imperfections, inverting U trivially leads one back to the initial state. The situation is more interesting when realistic imperfections are taken into account. We consider photon loss before U, between U and U^{-1}, and after U^{-1}, characterized by transmission coefficients η_1, η_2 and η_3 (see Figure 1). We will see that all three types of loss affect the entanglement, but it is clear that the loss between U and U^{-1} plays a special role, because it prevents the cancellation of U and U^{-1}. We are interested in the regime where the cancellation is still close to perfect, such that the final state in mode A is at the single-photon level, but may nevertheless contain significant vacuum and few-photon components. We therefore need an entanglement witness that can deal with these components. We use the entanglement criterion of ref. [157], which is based on that of ref. [164]. The state is proven to be entangled if

$$W = |\langle \vec{J}^A \cdot \vec{\sigma}^B \rangle| - \langle N^A \rangle > 0, \tag{2.5}$$

where $\vec{J}^A$ is the vector of Stokes operators for mode A, i.e. $J_z^A = a_h^\dagger a_h - a_v^\dagger a_v$, $J_x^A = a_0^\dagger a_0 - a_{0\perp}^\dagger a_{0\perp}$, $J_y^A = a_{\frac{\pi}{2}}^\dagger a_{\frac{\pi}{2}} - a_{\frac{\pi}{2}\perp}^\dagger a_{\frac{\pi}{2}\perp}$, where a_0, $a_{0\perp}$, $a_{\frac{\pi}{2}}$ and $a_{\frac{\pi}{2}\perp}$ are equatorial modes as introduced above; $\vec{\sigma}^B$ is the corresponding vector of Stokes operators for mode B, but restricted to the single-photon subspace; and $N^A = a_h^\dagger a_h + a_v^\dagger a_v$ is the total number of photons in A. Physically this corresponds to the fact that classically, $|\langle J_A . J_B\rangle| \leq |\langle J_A\rangle| |\langle J_B\rangle|$.

The multi-photon states generated by the cloning transformation U are quite complex [47, 157, 161]. It is therefore much more convenient to work in the Heisenberg picture, i.e. to transform the operators and evaluate their expectation values for the initial two-photon singlet state. Applying the appropriate sequence of beam splitter and squeezer operations corresponding to Figure 1, we find the overall transformation for any equatorial mode,

$$a' = \sqrt{\eta_1\eta_2\eta_3}\, a + \sqrt{(1-\eta_1)\eta_2\eta_3}\, c_1 + $$
$$\sqrt{(1-\eta_2)\eta_3}(\cosh(g)\, c_2 - \sinh(g)\, c_2^\dagger) + \sqrt{1-\eta_3}\, c_3, \tag{2.6}$$

9

where a' is the final mode, a is the initial mode, c_1, c_2, c_3 are the vacuum modes injected into the system by the losses before, in between, and at the end (see Figure 1); $g = \chi t$ is the gain of the cloner (and of the inverted cloner). The first term corresponds to when the photon transmits through all the beam-splitters which has an amplitude of $\sqrt{\eta_1 \eta_2 \eta_3}$. Similarly the second and the last term corresponds to the cases where the photon is lost on the first beam-splitter and when it is lost on the last one respectively. The interesting case is when the photon is lost on the second beam-splitter between the U and U^{-1}. In this case the vacuum fluctuations injected in the second beam-splitter are amplified with U^{-1} which gives the second term in Eq. (2.6). One can see that c_1 and c_3 just cause loss. In contrast the vacuum fluctuations due to c_2 are amplified by the second (inverting) cloner. This shows clearly that the intermediate loss is particularly important in the present context.

In order to calculate expectation values in the Heisenberg picture we also need the initial state. It is given by Eq. (2.1), which corresponds to the vacuum state for all the loss modes. It is helpful to rewrite it in terms of equatorial modes a and $a_\perp$ as $|\psi_-\rangle = \frac{1}{\sqrt{2}}(a^\dagger b_\perp^\dagger - a_\perp^\dagger b^\dagger)|\Omega\rangle$, using the simplified notation that we introduced after Eq. (2.4). The final mean photon number in A is

$$\langle\psi_-|N^A|\psi_-\rangle = \langle 1|a'^\dagger a'|1\rangle + \langle 0|a'^\dagger a'|0\rangle =$$
$$\eta_1 \eta_2 \eta_3 + 2(1-\eta_2)\eta_3 \sinh^2(g), \tag{2.7}$$

where $|0\rangle$ and $|1\rangle$ are the zero-photon and one-photon states for the initial mode a. We are interested in the regime where the transmission factors η_i are all fairly close to one (with η_2 very close to one, see below), such that the $\eta_1 \eta_2 \eta_3$ term in Eq. (2.7) is of order one, and where $2(1-\eta_2)\eta_3 \sinh^2(g)$ is small compared to $\eta_1 \eta_2 \eta_3$, such that the final state in A is again at the single-photon level. That is, the regime where the effect of the amplified vacuum fluctuations discussed above is relatively small.

Turning now to the question of entanglement in the final state, using Eq. (2.6) we get

$$\langle\psi_-|J_x^A \sigma_x^B|\psi_-\rangle = \langle\psi_-|J_y^A \sigma_y^B|\psi_-\rangle =$$
$$-\left(\langle 1|a'^\dagger a'|1\rangle - \langle 0|a'^\dagger a'|0\rangle\right) = -\eta_1 \eta_2 \eta_3. \tag{2.8}$$

Furthermore

$$\langle\psi_-|J_z^A \sigma_z^B|\psi_-\rangle = -\eta_1 \eta_2 \eta_3. \tag{2.9}$$

Note that J_z^A commutes with H and is thus not affected by the cloners at all. Putting all these pieces together, one finds

$$W = 2\left(\eta_1 \eta_2 - (1-\eta_2)\sinh^2(g)\right)\eta_3. \tag{2.10}$$

From Eq. (2.10) one can see that different loss channels have quite different effects on the entanglement witness, as was to be expected following the discussion after Eq. (2.6). Loss after the second cloner affects both terms equally and is thus relatively benign. The value of the witness just decreases proportionally to the transmission η_3. Loss before the first cloner reduces the first term, but only linearly in η_1. Note that this is in contrast to the situation for just one cloner, where loss before the cloner greatly affects the violation of the same entanglement criterion, see section VI.C of ref. [161]. This difference is due to the fact that in the present situation errors due to loss before the first cloner (which can be viewed as fluctuations due to the injected vacuum mode) are amplified by the first cloner, but de-amplified by the second one. The main problem in the present situation is loss between the two cloners, characterized by η_2. Errors due to this intermediate loss are amplified by the second cloner by a factor $\sinh^2(g)$. The size of this amplification is directly related to the mean number of photons (clones) after the first cloner, which is

$$N_c^A = \langle \psi_- | \tilde{a}^\dagger \tilde{a} | \psi_- \rangle = 2(1 + \eta_1) \sinh^2(g) + \eta_1, \qquad (2.11)$$

where the subscript c is for "clones" and $\tilde{a} = (\sqrt{\eta_1} a + \sqrt{1 - \eta_1} c_1) \cosh(g) + (\sqrt{\eta_1} a^\dagger + \sqrt{1 - \eta_1} c_1^\dagger) \sinh(g)$.

Eqs. (2.10) and (2.11) give

$$W = \frac{\eta_1(1 + \eta_2 + 2\eta_1\eta_2)\eta_3}{1 + \eta_1} - \frac{(1 - \eta_2)\eta_3}{1 + \eta_1} N_c^A. \qquad (2.12)$$

The negative term in this expression for W is proportional to both $(1 - \eta_2)$ and N_c^A. This implies that in order to prove entanglement using the witness W for increasing intermediate numbers of clones N_c^A, the transmission η_2 has to be closer and closer to one. This is illustrated in Figure 2. This probably rules out detecting entanglement for photon numbers of order 10^4, as in the experiment of ref. [47]. Supplementary assumptions thus would still have to be made in order to prove entanglement for such large photon numbers, see also the discussion in the introduction and refs. [47, 157, 161, 168, 167, 139] . However, the approach described here should allow to demonstrate entanglement for photon numbers much bigger than one without any additional assumptions, see Figure 2. Using anti-reflection coatings it should be possible to keep the losses between the two cloners, i.e. $1 - \eta_2$, at the level of at most a few percent. The transmission "before", η_1, is equivalent to the heralding efficiency for single-photon sources based on parametric down-conversion, for which values as high as 0.83 have been reported [135]. The transmission "after", η_3, is mainly limited by the detection efficiency, for which values as high as 0.95 have been achieved using transition-edge sensor detectors [112]. In Figure 2 we have conservatively assumed $\eta_1 = \eta_3 = 0.8$.
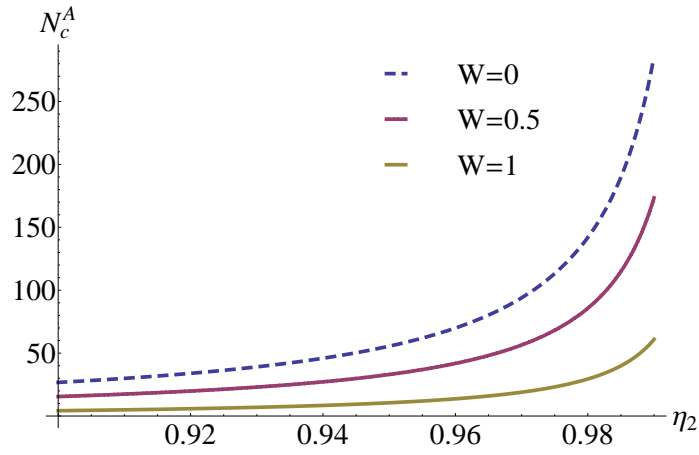
Figure 2.2: The number of clones after the first cloner N_c^A for which the entanglement witness W for the final state takes values 0, 0.5, 1 (from top to bottom), as a function of the intermediate transmission η_2, for fixed $\eta_1 = \eta_3 = 0.8$. Points below the top curve correspond to entanglement. Note that the theoretical maximum value for the witness is 2. As a consequence of Eqs. (9-10), proving entanglement is more difficult for larger numbers of clones in the intermediate state (i.e. for higher gain), requiring values of η_2 increasingly close to 1.

The figure shows that micro-macro entanglement involving a hundred photons or more on the macro side should be provable with the present approach, which therefore provides a new avenue for proving micro-macro entanglement without supplementary assumptions.

The high sensitivity to the transmission η_2 (in the high photon-number regime) shown here is closely related to the results of refs. [167] and [139], which show that the detectable micro-macro entanglement is highly sensitive to loss (for a homodyne measurement) and coarse-graining (for photon counting measurements) respectively. Let us note that micro-macro entanglement is present even for small values of η_2 (i.e. large loss), at least for the simple model used in this paper. This follows from the results of ref. [157], where the same entanglement witness that we use here was applied directly to the micro-macro state. However, the presence of this entanglement can be proved experimentally only by very difficult measurements, which involve counting large photon numbers with single-photon level resolution [139].

2.3   Applications

So far we have discussed the proposed experiment from a purely foundational point of view, as a way to demonstrate information preservation in quantum cloning and the existence of micro-macro entanglement. We now argue that it might also be interesting from a much more applied perspective. Detecting small variations in transmission across a sample is one of the most fundamental problems in optical imaging. For example, biological samples often have very low contrast, see e.g. [131] for more details. The standard approach is to use a classical beam of light (corresponding to a coherent state in the quantum description) and measure the variation of the transmitted intensity. However, a coherent state has a Poissonian photon number distribution, which implies that it has photon number fluctuations of $\sqrt{N}$, for a mean number of photons N in the beam. This means that a small change in transmission $\Delta\eta$ is only observable if $N\Delta\eta > \sqrt{N}$, or $\Delta\eta > \frac{1}{\sqrt{N}}$. For small $\Delta\eta$ one thus requires quite large N, which can be a problem for highly light-sensitive samples (e.g. living cells).

In contrast, consider a situation where the sample is placed between the first and second cloner in Figure 2. Eq. (2.12) implies that W varies strongly with a change in η_2,

$$\frac{dW}{d\eta_2} = \frac{\eta_3}{1+\eta_1}N_c^A + \frac{\eta_1\eta_3(1+2\eta_1)}{1+\eta_1}. \tag{2.13}$$

The first term dominates over the second one even for quite modest intermediate photon numbers N_c^A. This means that $\frac{dW}{d\eta_2}$ is *linear* in the total number of photons N_c^A transmitted

through the sample. For comparison with the above discussion of the coherent-state case we will refer to this number as $N \equiv N_c^A$. The smallest detectable change $(\Delta\eta_2)_{min}$ is given by $(\Delta W)_{min}/(\frac{dW}{d\eta_2})$, where $(\Delta W)_{min}$ is the smallest detectable change in W. Under typical experimental conditions $(\Delta W)_{min}$ will depend on the precision of the experiment and on the number of repetitions, but it will be independent of N. As a consequence, for large enough N, $(\Delta\eta_2)_{min}$ scales like $\frac{1}{N}$, compared to $\frac{1}{\sqrt{N}}$ in the case of the coherent state. This much more advantageous scaling is a quantum enhancement that is due to the use of entangled light. It is analogous to the Heisenberg limit (in contrast to the standard quantum limit) in interferometry [71, 56]. This suggests that the present approach may be promising as a quantum measurement technique.

Chapter 3

Precision requirements for observing macroscopic quantum effects

Most of the content of this chapter was published in [180]. I contributed to the main ideas and the calculations in this work. Specifically, I did some of the calculations and double checked the rest of them.

3.1   Introduction

What are the requirements for observation of macroscopic quantum effects such as Schrödinger's cat? Although isolation and avoiding decoherence is necessarily [192], there are results that show that this is not enough and the precision of the measurements also plays a significant role.

In 1980 Mermin [118] showed that for a Bell inequality violation with a singlet state of two large spins s, the required angular resolution of the directions of the spin measurements increases with the size of the spins as $1/s$. This is an example for necessary measurement *control precision*, i.e. the precision with which relevant physical parameters have to be controlled in order to implement the desired measurement procedure.

Later Peres [132] showed that not only the control precision, but also the precision with which the measurement outcomes are known is also important. He showed that quantum predictions for the correlation functions can be reproduced from a classical model if the measurement *outcome precision* is worse than $O(\frac{1}{\sqrt{s}})$ in relative terms, i.e. if the measurement error Δm grows faster with than $O(\frac{1}{\sqrt{s}})$, then the outcome can be reconstructed

classically. Similar results were obtained for single spin in Ref. [94]. Ref. [164] studied multi-photon singlet states equivalent to Mermin's and Peres' spin singlets and showed that $O(\frac{1}{\sqrt{N}})$ relative outcome precision (where N is the photon number) is sufficient to demonstrate entanglement. Most recently Ref. [139] studied so-called micro-macro entangled states of light that are obtained by greatly amplifying one half of an initial entangled photon pair. They found that a relative outcome precision of order $\frac{1}{N}$ was necessary to see quantum effects in this case. Similar results on the effect of coarse-graining on macroscopic entanglement were reported in Refs. [168, 178, 167, 136].

Ref. [139] also conjectured that demonstrating quantum effects in macroscopic systems always requires high measurement precision. However, there is a proposal in [87] that is in contrast with this conjecture. In this proposal, Kerr non-linearities is exploited to get a Bell inequality violation for macroscopic state with coarse-grained measurements. Ref. [139] pointed out that the non-linear operations used in this proposal involve large (π) phase shifts between neighbouring Fock states which could be seen as high resolution in a more general sense. It was shown in Ref. [70, 179] that in order to prepare entangled states in the proposal of Ref. [87], the phase of the non-linear operations has to be controlled with a precision that increases with system size. Ref. [70, 179] is linked to the present work in that it already highlighted the importance of phase precision. However, it focused on state preparation. Here we explicitly address the question of measurement precision posed in Ref. [139]. We show that even if one assumes that the states under consideration are ideal, measurement precision - in particular control precision - has to increase with system size in order to be able to demonstrate quantum effects.

3.2 Macroscopic Superpositions: Requirement for High Outcome Precision

We study superpositions and entanglement involving coherent states with opposite amplitudes, $|\alpha\rangle$ and $|-\alpha\rangle$, where we will take α to be real for simplicity. We will pay particular attention to the macroscopic limit $\alpha \gg 1$. We study this example not only because these states lie at the heart of the proposal of Ref. [87], but also because they are a well-known "archetype" for macroscopic quantum superpositions [189, 24, 120, 129, 5, 91]. Let us note right away that the proposal of Ref. [87] is more complex than the simple cases considered here. However, our conclusions concerning control precision apply to that work as well. We focus on simple states and measurement schemes for clarity.

We begin by considering the superposition state

$$|\alpha_+\rangle = \frac{1}{\sqrt{2}}(|\alpha\rangle + i|-\alpha\rangle), \tag{3.1}$$

focusing on the regime where α is large enough such that the overlap $\langle\alpha|-\alpha\rangle = e^{-2\alpha^2}$ is negligible. The phase factor i is chosen for convenience. This state can be created, for example [189, 91], from an initial coherent state with the help of a Kerr nonlinearity,

$$e^{-i\frac{\pi}{2}\hat{N}^2}|\alpha\rangle = e^{-i\frac{\pi}{4}}|\alpha_+\rangle, \tag{3.2}$$

where $\hat{N} = a^\dagger a$, and a is the bosonic annihilation operator for which the coherent state is an eigenstate, $a|\alpha\rangle = \alpha|\alpha\rangle$. It was shown in Ref. [70, 179] that the phase of the unitary operation in Eq. (3.2) has to be precisely equal to $\frac{\pi}{2}$ in order to generate this state with high fidelity, with a precision that increases with α. However, as mentioned in the introduction, this is not our concern here. We will assume that the ideal state is given to us and focus on the question of how to prove that we have a quantum superposition state, as opposed to a "classical" mixture of the same two coherent states,

$$\rho = \frac{1}{2}(|\alpha\rangle\langle\alpha| + |-\alpha\rangle\langle-\alpha|). \tag{3.3}$$

Let us first consider measurements of the quadrature $\hat{x} = \frac{1}{2}(a + a^\dagger)$. For the state of Eq. (3.1), this will give a symmetric bimodal distribution of results corresponding to the two components of the superposition,

$$P(x) = |\langle x|\alpha_+\rangle|^2 = \frac{e^{-(x+\alpha)^2} + e^{-(x-\alpha)^2}}{2\sqrt{\pi}}, \tag{3.4}$$

where $\hat{x}|x\rangle = x|x\rangle$. Note that for $\alpha \gg 1$ one can distinguish the two components using very coarse-grained measurements of $\hat{x}$; this point will be significant below. However, this does not prove that one is dealing with a macroscopic superposition state, since the mixed state of Eq. (3.3) will produce the exact same distribution of outcomes. Often, one has to measure at least two *non-commuting* observables in order to prove the quantum character of any system. One obvious choice for an observable that does not commute with $\hat{x}$ is the complementary quadrature, $\hat{p} = \frac{-i}{2}(a - a^\dagger)$. The probability distribution of the associated outcomes p is

$$P_{|\alpha+\rangle}(p) = |\langle p|\alpha_+\rangle|^2 = \frac{e^{-p^2}(1 - \sin(2\alpha p))}{\sqrt{\pi}} \tag{3.5}$$
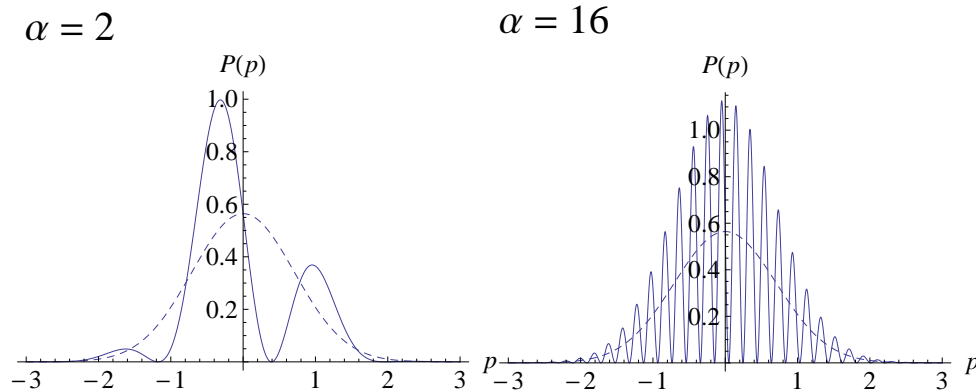
Figure 3.1: Probability of outcomes for measurements of the $\hat{p}$ quadrature for the super-position state of Eq. (3.1) and the mixed state of Eq. (3.3) for $\alpha = 2$ (left) and $\alpha = 16$ (right). The oscillatory structure that distinguishes the two distributions becomes harder to resolve as α increases, see also Eqs. (3.5) and (3.6).

where $\hat{p}|p\rangle = p|p\rangle$, whereas for the mixed state of Eq. (3.3) one has

$$P_\rho(p) = \langle p|\rho|p\rangle = \frac{e^{-p^2}}{\sqrt{\pi}}. \tag{3.6}$$

The two probability distributions are different, which means that the measurement of $\hat{p}$ can indeed be used to discriminate Eq. (3.1) from Eq. (3.3). However, the difference is due to the oscillatory term in Eq. (3.5), whose oscillation frequency increases with increasing α. Detecting this oscillation therefore requires a precision in the $\hat{p}$ measurement that increases with α, see also Fig. 3.1. In fact, this was one of the examples mentioned in Ref. [139] in order to argue for the plausibility of the considered conjecture. The same effect can also be discussed in terms of the Wigner function [191]. Fig. 3.1 could also be compared to Fig. 2 of Ref. [139], which shows a similar effect for a different macroscopic quantum state.

3.3 Nonlinear Rotations of Coherent-State Qubits: Requirement for High Control Precision

There is a different approach to proving the superposition character of $|\alpha_+\rangle$, which is closely linked to the proposal of Ref. [87]. One can view the states $|\alpha\rangle$ and $|-\alpha\rangle$ as the computational basis states of a "coherent state qubit" [35, 125, 85]. Measurements
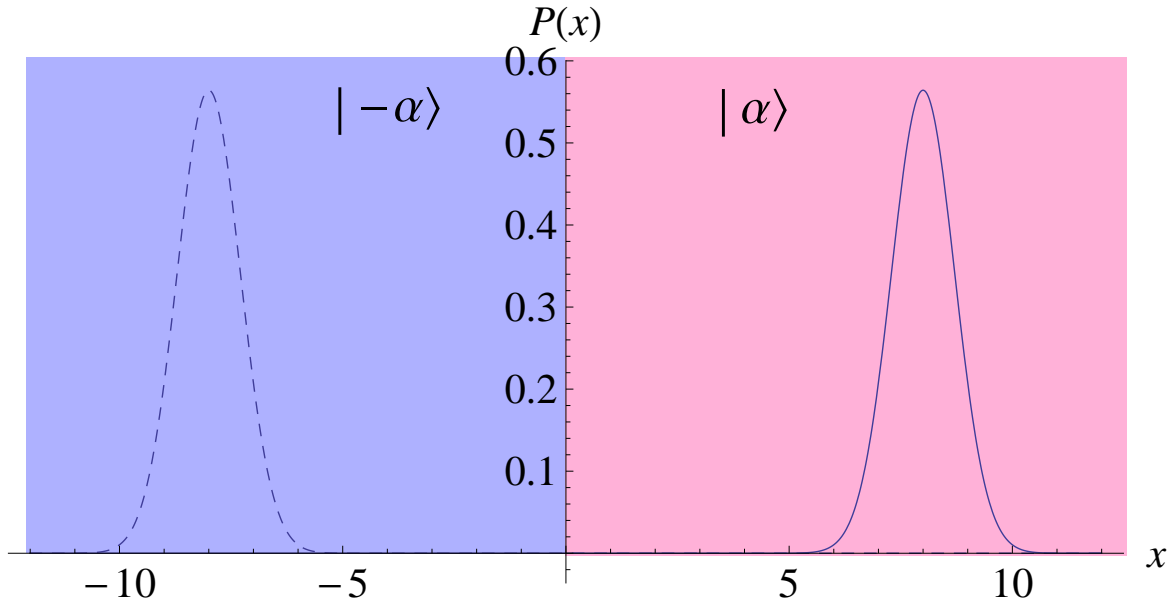
Figure 3.2: Outcome distributions for measurements of the $\hat{x}$ quadrature for the states $|\alpha\rangle$ (solid) and $|-\alpha\rangle$ (dashed) for $\alpha = 8$. For large enough α, the two states can be distinguished by a very coarse-grained measurement. Positive values (red) of $\hat{x}$ can be assigned to $|\alpha\rangle$ and negative values (blue) to $|-\alpha\rangle$. The overlap between the two distributions, and thus the error of this measurement scheme, is negligible.

in the computational basis, which we will also refer to as σ_z measurements (where $\sigma_z = |\alpha\rangle\langle\alpha| - |-\alpha\rangle\langle-\alpha|$), can clearly be done in a very coarse way, e.g. by measuring $\hat{x}$. For large enough α, positive (negative) values correspond to the state $|\alpha\rangle$ ($|-\alpha\rangle$) with extremely high fidelity, and coarse-graining the x values only has a negligible effect on the measurement fidelity, see also Fig. 3.2.

As before, proving the quantum character of (3.1) requires at least one other measurement that does not commute with σ_z. A natural choice from the qubit perspective is

$$\sigma_y = |\alpha_+\rangle\langle\alpha_+| - |\alpha_-\rangle\langle\alpha_-|, \tag{3.7}$$

where $|\alpha_-\rangle = \frac{1}{\sqrt{2}}(i|\alpha\rangle + |-\alpha\rangle)$. If σ_y can be measured, then it is obviously easy to prove that a given source produces the state Eq. (3.1) - the corresponding measurement will always give the result $+1$ and never -1, whereas for the mixed state (3.3) the results would be 50/50.
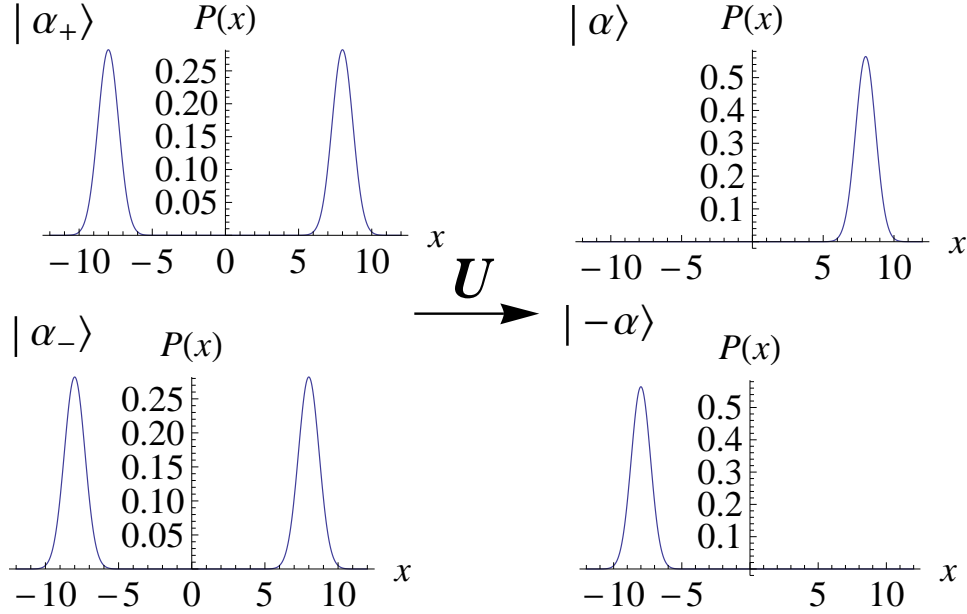
Figure 3.3: The $\hat{x}$ quadrature distributions for the states $|\alpha_+\rangle = \frac{1}{\sqrt{2}}(|\alpha\rangle + i|-\alpha\rangle)$ (top left) and $|\alpha_-\rangle = \frac{1}{\sqrt{2}}(i|\alpha\rangle + |-\alpha\rangle)$ (bottom left) are identical. However, application of the Kerr rotation Eq. (3.9) transforms $|\alpha_+\rangle$ into $|\alpha\rangle$ (top right) and $|\alpha_-\rangle$ into $|-\alpha\rangle$ (bottom right). These states can now be distinguished by a coarse-grained measurement as in Fig. 3.2.

The required measurement of σ_y can be implemented using a Kerr non-linearity, see also Ref. [85]. Changing the sign of α in Eq. (3.2) one has $e^{-i\frac{\pi}{2}\hat{N}^2}|-\alpha\rangle = e^{-i\frac{\pi}{4}}|\alpha_-\rangle$. Inverting these relations one sees that the Kerr operation allows one to rotate the σ_y eigenstates into the σ_z eigenstates, i.e.

$$U|\alpha_+\rangle = |\alpha\rangle, U|\alpha_-\rangle = |-\alpha\rangle, \tag{3.8}$$

where

$$U = e^{-i\frac{\pi}{4}}e^{i\frac{\pi}{2}\hat{N}^2}. \tag{3.9}$$

This means that a measurement of σ_y can be done on an arbitrary state by first applying the rotation U, followed by a measurement in the σ_z basis, as shown in Fig. 3.3. As mentioned before and in Fig. 3.2, the σ_z measurement can be done in a very coarse way. This means that it is possible to prove the presence of the macroscopic superposition (3.1) using measurements that are coarse in terms of outcome resolution.

However, we argue that it is physically important to also consider the necessary control precision. The control parameter that we focus on here is the phase of the Kerr rotation

U. Suppose that instead of exactly $\frac{\pi}{2}$ this phase is $\frac{\pi}{2} + \phi$. Then, when trying to perform the σ_y measurement, the state $|\alpha_+\rangle$ will be rotated not into $|\alpha\rangle$, but into $e^{i\phi\hat{N}^2}|\alpha\rangle$, and $|\alpha_-\rangle$ into $e^{i\phi\hat{N}^2}|-\alpha\rangle$. For simplicity let us consider a Gaussian distribution for ϕ with a width $\sigma \ll 1$ (which is the relevant regime, as will become clear below). Note that a constant wrong angle, would lead to simple bit-flip error because it creates components of the orthogonal state. Then the final state corresponding to $|\alpha_+\rangle$ is

$$C_\sigma(|\alpha\rangle\langle\alpha|) = \frac{1}{\sqrt{2\pi}\sigma} \int_{-\infty}^{\infty} d\phi e^{-\frac{1}{2}\frac{\phi^2}{\sigma^2}} e^{i\phi\hat{N}^2}|\alpha\rangle\langle\alpha|e^{-i\phi\hat{N}^2} =$$
$$\frac{e^{-\alpha^2}}{\sqrt{2\pi}\sigma} \int_{-\infty}^{\infty} d\phi e^{-\frac{1}{2}\frac{\phi^2}{\sigma^2}} \sum_{n,n'=0}^{\infty} e^{i\phi(n^2-n'^2)} \frac{\alpha^{n+n'}}{\sqrt{n!}\sqrt{n'!}}|n\rangle\langle n'|, \qquad (3.10)$$

where we have introduced the notation C_σ for the associated error channel, extended the range of integration for ϕ to infinity (which can be done with negligible error for $\sigma \ll 1$), and expanded $|\alpha\rangle$ in terms of photon number states. Performing the integration over ϕ one finds

$$e^{-\alpha^2} \sum_{n,n'=0}^{\infty} e^{-\frac{1}{2}\sigma^2(n^2-n'^2)^2} \frac{\alpha^{n+n'}}{\sqrt{n!}\sqrt{n'!}}|n\rangle\langle n'|. \qquad (3.11)$$

The term containing σ leads to a suppression of the off-diagonal elements in the number state basis. The key point for the present work is that this suppression happens faster for larger values of α. This can be seen by remembering that the number distribution for a coherent state is a Poissonian with a peak at α^2 (and a corresponding width α). For large enough α one can then approximate the factor $(n^2 - n'^2)^2 = (n + n')^2(n - n')^2$ in the exponential in Eq. (3.11) by $4\alpha^4(n - n')^2$. This shows that the off-diagonal elements are suppressed by a Gaussian factor $e^{-2\sigma^2\alpha^4(n-n')^2}$. This means that for $\sigma\alpha^2 \gtrsim 1$ the state (3.11) is essentially diagonal in the number basis. Moreover the state corresponding to $|\alpha_-\rangle$, which we denote $C_\sigma(|-\alpha\rangle\langle-\alpha|)$, converges to the same diagonal form. In this regime there is therefore no way to distinguish these two states, see also Fig. 3.4.

This means that the described procedure for measuring σ_y breaks down for phase errors σ that are of order $\frac{1}{\alpha^2}$, or $\frac{1}{N}$, if $N = \alpha^2$ is used to denote the typical number of particles in the system. The precision with which ϕ has to be controlled thus increases with system size. The coherent state qubit approach relies on being able to confine the dynamics of the system to the two-dimensional subspace spanned by $|\alpha\rangle$ and $|-\alpha\rangle$, even though the number of Fock states that effectively contribute to the dynamics is of order α (due to the Poisson distribution of numbers for coherent states). This becomes more and more difficult for increasing α. The evolution of coherent states under small Kerr rotations is discussed also in different terms in Refs. [92, 80].
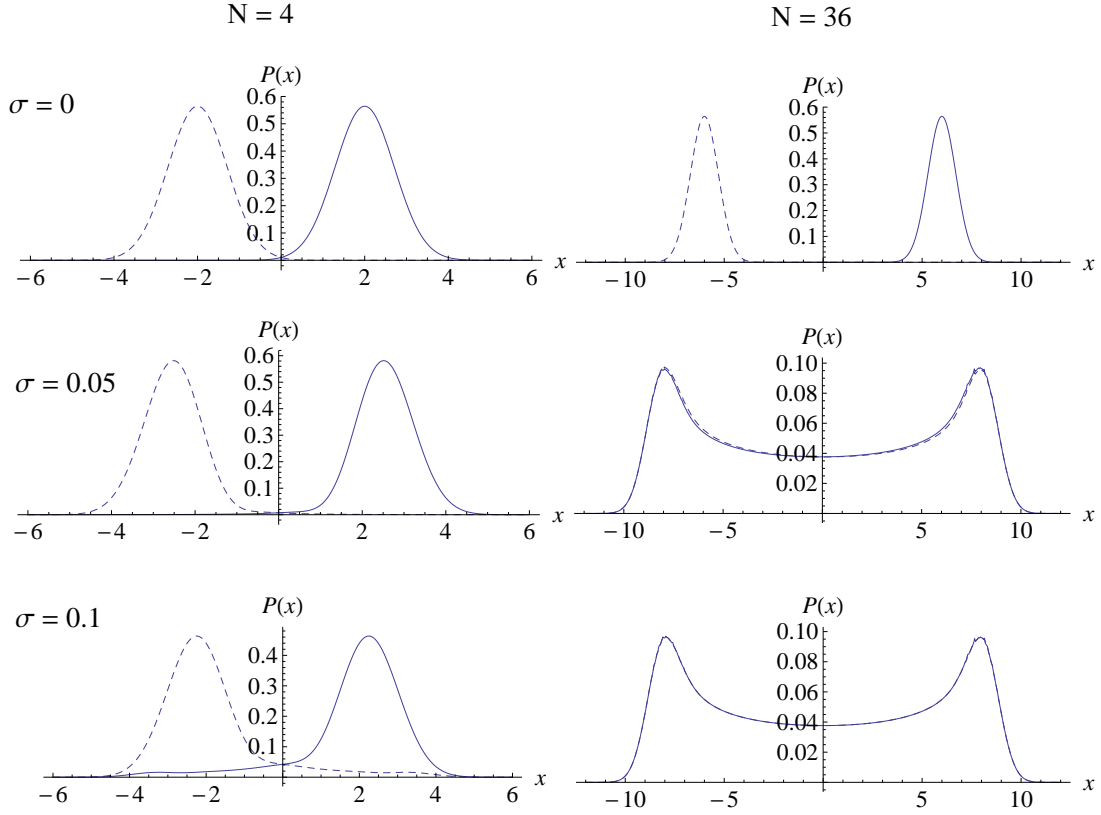
Figure 3.4: Outcome distributions for $\hat{x}$ quadrature measurements for the states $C_\sigma(|\alpha\rangle\langle\alpha|)$ (solid) and $C_\sigma(|-\alpha\rangle\langle-\alpha|)$ (dashed) that are created from the states $|\alpha_+\rangle$ and $|\alpha_-\rangle$ by a Kerr rotation with Gaussian phase uncertainty σ, see Eq. (3.10). We show the case $N = \alpha^2 = 4$ on the left and $N = 36$ on the right, with σ increasing from top to bottom. One sees that the distributions overlap much faster for greater N, leading to errors in the σ_y measurement of Fig. 3.3, see also Fig. 3.2. For large enough σ it becomes impossible to distinguish the two states.
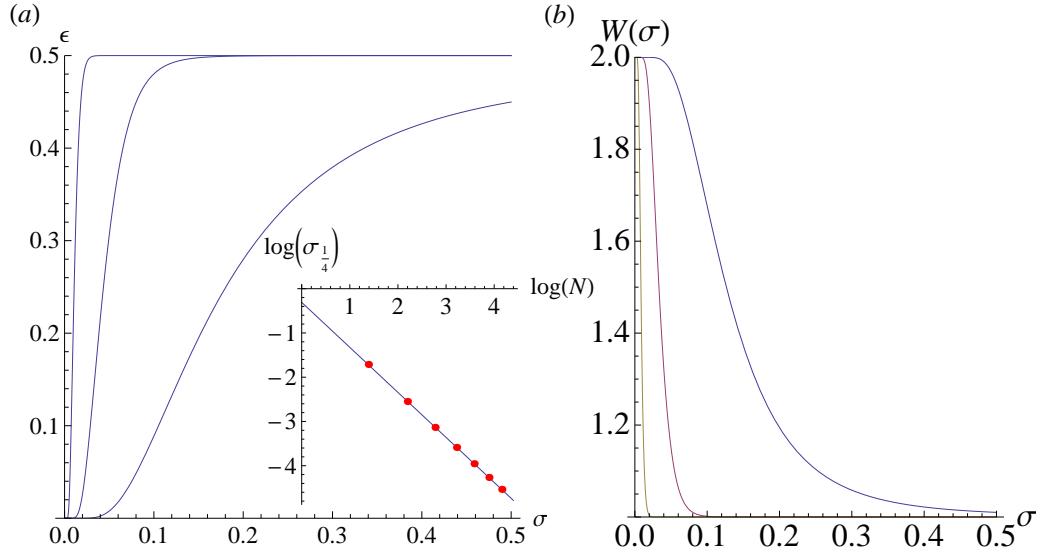
Figure 3.5: (a) The bit-flip error ϵ in the σ_y measurement of Fig. 3.3 as a function of the Kerr phase uncertainty σ, for the cases $N = \alpha^2 = 4, 16, 64$ from bottom to top. One sees that ϵ approaches $\frac{1}{2}$ for increasing σ, and this happens faster for greater N. The log-log plot in the inset shows that the value of σ for which $\epsilon = \frac{1}{4}$ (i.e. half its asymptotic value) scales like $\frac{1}{N}$, as expected from the analytical argument given in the text. (b) Expectation value of the entanglement witness W of Eq. (3.13) for the state of Eq. (3.12), for $N = \alpha^2 = 4, 16, 64$ from top to bottom in blue, red and yellow respectively. For increasing σ the value of W approaches 1 (the bound for separable states), due to the bit-flip errors in the σ_y measurement shown in (a). This happens faster for greater values of N.

This result holds no matter how the final measurement in the σ_z basis is performed. For concreteness, we show in Figs. 3.4 and 3.5(a) how the phase error σ affects the measurement strategy described in Figs. 3.3 and 3.2. Fig. 3.4 shows that the $\hat{x}$ quadrature distributions for the states $C_\sigma(|\alpha\rangle\langle\alpha|)$ and $C_\sigma(|-\alpha\rangle\langle-\alpha|)$ begin to overlap for increasing σ, and that this happens much faster for greater values of α. Fig. 3.5(a) shows the resulting bit-flip error ϵ for the σ_y measurement of Fig. 3.3. This can be calculated as $\epsilon = \int_{-\infty}^{0} dx\, P(x)$, with $P(x)$ the $\hat{x}$ quadrature distribution for the state $C_\sigma(|\alpha\rangle\langle\alpha|)$. As expected from the above discussion, ϵ approaches $\frac{1}{2}$ (corresponding to complete indistinguishability of the two states) for increasing σ, and this happens faster for greater values of α.

3.4   Macroscopic Entanglement

So far we have discussed macroscopic superposition states. We now turn to the detection of macroscopic entanglement. Consider the state

$$|\Phi_-\rangle = \frac{1}{\sqrt{2}}(|\alpha\rangle|\alpha\rangle - |-\alpha\rangle|-\alpha\rangle), \tag{3.12}$$

where the relative sign between the two terms is chosen for convenience. This state can be created, for example, using a Kerr non-linearity, combined with a beam splitter and phase space displacements [70, 179, 85, 150, 151]. Again our focus here is not on how to create the state, but on whether its entanglement can be demonstrated by coarse-grained measurements.

As before, coarse quadrature measurements alone are not sufficient, but the coherent state qubit approach using the Kerr nonlinearity can be applied to the present case as well. Again measurements only in the computational basis (σ_z) are not sufficient to distinguish the entangled state (3.12) from a separable state, in particular from the 50/50 mixture of the product states $|\alpha\rangle|\alpha\rangle$ and $|-\alpha\rangle|-\alpha\rangle$. However, the entanglement can be demonstrated using the witness operator

$$W = \sigma_y \otimes \sigma_y + \sigma_z \otimes \sigma_z. \tag{3.13}$$

One easily verifies that $\langle\Phi_-|W|\Phi_-\rangle = 2$, whereas the modulus of the mean value of W for separable states is bounded by one. This follows from the fact that for any state $|\chi\rangle$ the norm of the two-dimensional vector $\{\langle\chi|\sigma_y|\chi\rangle, \langle\chi|\sigma_z|\chi\rangle\}$ is bounded by one. For any product state, the mean value of W is the scalar product of two such vectors, and its modulus is therefore also bounded by one; and every separable state is a convex combination of product states, thus satisfying the same bound, see also Ref. [51]. This witness can be turned into a conventional witness simply by using $1 - W$.

By performing measurements of σ_z and σ_y on each subsystem one can therefore prove the entanglement in the state (3.12). As discussed above, a coarse-grained measurement of the $\hat{x}$ quadrature, for example, is sufficient to do the σ_z measurement, but the σ_y measurement requires moreover the Kerr rotation (3.9). Therefore the exact same control precision requirements as above apply here as well. We showed in Fig. 5(a) that for a phase error $\sigma \gtrsim \frac{1}{\alpha^2}$, the bit-flip error ϵ in the σ_y measurement approaches $\frac{1}{2}$. The measured mean value of W, which is equal to $1+(1-2\epsilon)^2$ (as can easily be shown, assuming that the σ_z measurement is perfect), therefore tends to 1, see also Fig. 3.5(b). This means that the macroscopic entanglement becomes increasingly hard to detect as α increases. Note that as long as the mean value is greater than one, entanglement can in principle be proven. Our main point here is the scaling with α. Due to this scaling, for any given non-zero level of experimental imperfection, there is a system size above which entanglement is no longer measurable.

3.5   Conjecture and Discussion

We have seen that using macroscopic "coherent state qubits" one can in principle observe macroscopic quantum features such as superposition and entanglement using measurements that are very coarse in terms of outcome precision. However, there is a price to be paid. The measurements rely on being able to perform a rotation of the macroscopic qubit basis. When this rotation is implemented using a Kerr non-linearity, the control precision of the Kerr phase shift has to increase with the size of the system. The apparent counter-example of Ref. [87] has thus led us to a refined formulation of the conjecture of Ref. [139] that is both more precise and more general: the measurement precision required for demonstrating macroscopic quantum effects seems to increase with the size of the system, provided that both outcome precision and control precision are taken into account. This could be compared, for example, to the results of Ref. [95], which studied the effect of coarse graining on macroscopic realism as defined by Leggett [110] and emphasized the computational complexity (rather than the precision) of the operations that were required to observe violations of macroscopic realism.

The above conjecture is attractive, but it is far from proven. Different parts of our argument have a different degree of generality. The requirement for a rotation from a macroscopic superposition basis to a "computational" basis is very general in the present context. On the one hand, for a coarse-grained measurement approach to work there has to be one basis for which the relevant states are easy to distinguish. On the other hand, to prove quantum characteristics one also has to be able to measure at least one observable

that corresponds to a different basis, hence the need for a rotation between that basis and the computational basis. As a simple extension, one might want to consider other superposition states or entangled states using the same coherent-state qubits. Proving superpositions or entanglement then requires slightly different rotations. More general qubit basis rotations can be constructed out of the Hadamard-type rotation U of Eq. (3.9) and phase space displacements [85]. The same control precision requirements apply for this construction. They also apply to the measurements proposed in Ref. [87].

But could there be other ways of performing the basic Hadamard rotation? Do they necessarily have the same control precision requirements? In fact, it is known that the Kerr non-linearity is not the only possible solution [189]. Higher powers of $\hat{N}^2$ also work. However, by adapting the argumentation around Eqs. (3.10,3.11) to these cases one can easily show that the control precision requirements are only increased in this case. For a Hamiltonian proportional to $\hat{N}^{2k}$ the necessary control precision scales as $\frac{1}{N^{2k-1}}$. So the Kerr non-linearity is optimal at least for this family of possible approaches.

We suggest that the basic difficulty with implementing a macroscopic basis rotation of the type of Eq. (3.9) stems from the fact that the underlying Hilbert space is very large. In our case the effective Hilbert space dimension is of order α, corresponding to the range of photon numbers that have significant weights for a coherent state. For increasing α it requires more and more fine-tuning to perform a non-trivial operation on the states $|\alpha\rangle$ and $|-\alpha\rangle$, while confining them to the two-dimensional subspace that they span. This may be a generic difficulty for macroscopic quantum systems.

We feel that proving these conjectures and intuitions would be very interesting, as it would significantly advance our understanding of the macroscopic limit of quantum physics. It would possibly be even more interesting if one could find a counter-example, since the latter might provide a promising avenue towards the demonstration of truly macroscopic quantum effects.

Chapter 4

The Asymptotic Cooling of Heat-Bath Algorithmic Cooling

Most of the content of this chapter was published in [138]. I proposed the main idea of the paper, found the solution and did all of the calculations. I also contributed in writing the paper.

4.1 Overview

The purity of quantum states is a key requirement for many quantum applications. Improving the purity is limited by fundamental laws of thermodynamics. Here we are probing the fundamental limits for a natural approach to this problem, namely heat-bath algorithmic cooling (HBAC). The existence of the cooling limit for HBAC techniques was proved by Schulman et al. [153] A bound for this value was found by Elias et al. [53] and numerical testing supported the hypothesis that their bound may be the actual limit. A proof or disproof of whether their bound was the actual limit remained open for the past decade. Here for the first time we prove this limit. In the context of quantum thermodynamics, this corresponds to the maximum extractable work from the quantum system. We also establish, in the case of higher dimensional reset systems, how the performance of HBAC depends on the energy spectrum of the reset system.

4.2 Introduction

The purity of quantum states is often one of the limiting factors in many applications and quantum technologies. For instance, the signal to noise ratio (SNR) in spectroscopy and medical imaging [4, 78, 99, 127, 147] or the resolution in metrology and quantum sensing [123, 171, 144, 188] are often limited by the purity of the quantum states. High purity is also a necessity for quantum computation. Fault-tolerant quantum computing relies on using fresh ancillary quantum bits. Recently Ben-Or, Gottesman and Hassidim proposed a quantum refrigerator to prepare high purity quantum states for this purpose using algorithmic cooling [13].

Different methods have been exploited to improve the purity but all of these techniques are limited by the laws of thermodynamics [83, 1]. It is interesting both fundamentally and practically to understand these limits. In the context of quantum thermodynamics, extracting work from a quantum system is equivalent to increasing its purity and cooling it [82] and cooling limits correspond to Carnot-like efficiency limits. Quantum thermodynamics has been studied as a resource theory of purity [82, 73, 19] and recently Horodecki and Oppenheim extended this paradigm for general thermodynamic transformations. They found the limit for the extractable work in terms of relative entropy when the Hamiltonian of the process is time independent. Usually quantum applications involve quantum control which means that the Hamiltonian is time-dependent, and in these cases their result gives an upper bound.

Heat-bath algorithmic cooling is another method which takes a more practical approach to the cooling problem. Here a natural subclass of general thermodynamic transformations is considered where we have control over a part of the system, and have limited control over how the system interacts with an external heat-bath [1, 181]. This model applies to a wide range of quantum implementation techniques like nuclear magnetic resonance (NMR) [148, 9, 21], ion-traps [7] and recently in quantum optics [186]. The HBAC methods have also been studied from the thermodynamic viewpoint [143, 181].

4.2.1 Model

We consider a quantum system that is in interaction with a heat-bath. The quantum system comprises two kind of qubits, the computation qubits and the reset qubits. The computation qubits are the high quality qubits with long decoherence time that are used for computation. The reset qubits on the other hand have shorter relaxation time and equilibrate fast. Figure 4.1 shows a schematic of the model that we are considering in our
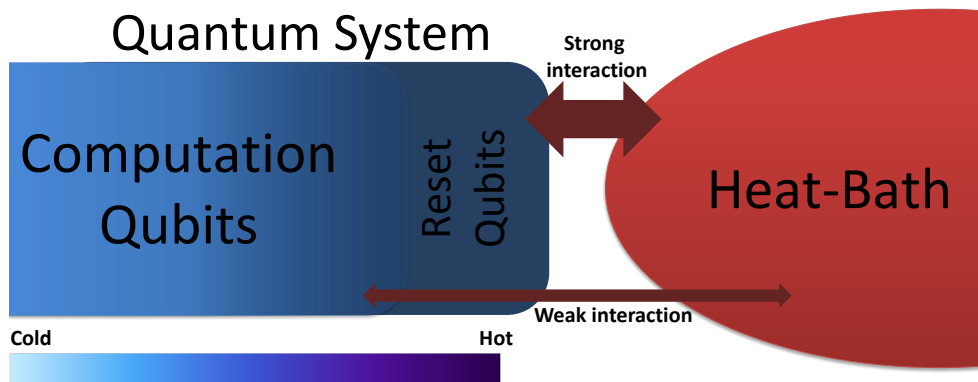
Figure 4.1:   The schematic of the model. The quantum system comprises computation qubits and reset qubits and interacts with a heat-bath. The heat-bath incorporates degrees of freedom in the environment that couple to the qubits in the quantum system. Usually, different qubits couple differently to these degrees of freedom. The computation qubits interact weakly and the reset qubits interact strongly with the heat-bath. We ignore the weak interaction between the computation qubits and the heat-bath and assume that only the reset qubits are effected by the interaction with the heat-bath. The goal is to cool down the qubits in the system. Note that this is just a schematic and in reality they are not necessarily spatially arranged in this way. The HBAC does not cool all the qubits to the same temperature and the asymptotic temperature of different computation qubits would be different. We find the asymptotic state and consequently the temperature for all the qubits including the first one which is the cooling limit for all the HBAC techniques. Note that the heat-bath is hotter than the system which is indicated by the red color.

work. Thus, the HBAC model does not consider the possibility of irreversible operations on the computation system (other than interacting reversibly with the reset system).

This model applies to a variety of physical systems. For instance, in NMR, the system is the few nuclear spins that can be controlled and the heat-bath comprises the other magnetic moments in the sample. These magnetic moments couple to the nuclear spins in the system and eventually equilibrate them. Different spin species have different coupling rates [148, 9].

4.2.2   Heat-bath Algorithmic Cooling

The class of cooling transformations that we are considering here are known as heat-bath algorithmic cooling [17, 153, 9]. HBAC is a quantum computation technique for cooling

computation qubits by transferring their entropy to the reset qubits. The reset qubits are regularly refreshed through their interaction with the heat-bath.

The original idea of algorithmic cooling was developed by Schulman and Vazirani in [155] which uses a technique for Schumacher's quantum data compression [34, 89]. Later it was proposed to use a heat-bath to enhance the cooling beyond the compression bounds[17, 59]. The idea is that after the entropy transfer, the heat-bath refreshes the hot qubits and then the entropy transfer can be repeated. Different iterative methods were developed based on this idea[53, 55, 89]. All of these methods are referred to as "Heat-Bath Algorithmic Cooling".

In [153] Schulman et al. established a lower-bound for the asymptotic temperature and proved that none of these iterative techniques can extract all of the entropy from the computation qubits. In [53], a steady state of HBAC was identified and was used to establish an upper bound for the limit under the assumption that HBAC starts from the maximally mixed state and converges to a steady state. They found numerical evidence that the bound was tight, however no proof of this limit was known.

In this work, we show that this process has an asymptotic state and find this asymptotic state of the computation and reset qubits. This gives the cooling limit of the qubits in this framework. This fundamental limit sets the ultimate limit of any practical cooling approach under similar constraints.

4.2.3   Partner Pairing Algorithm

We use the technique that was introduced in [153]. It is called the "Partner Pairing Algorithm (PPA)" and is the optimal technique for HBAC. We find the cooling limit for the PPA and as it is the optimal technique, the limit applies to all the HBAC techniques as well.

The PPA is an iterative method. In each iteration, the diagonal elements of the density matrix are sorted and then the reset qubit is refreshed. For example, if we have $n = 1$ computational qubits, plus one reset qubit, with combined probabilities corresponding to 0.45 for $|00\rangle$, 0.15 for $|01\rangle$, 0.3 for $|10\rangle$ and 0.1 for $|11\rangle$, then the sort step will swap $|01\rangle$ and $|10\rangle$. After this swap step, the probabilities of the computational basis states are in decreasing order with respect to the lexicographic ordering of the qubits, which corresponds to increasing the probability of a 0 in the leftmost qubit.

Reset process

The reset process is equivalent to

$$R(\rho) = \text{Tr}_R(\rho) \otimes \rho_R. \tag{4.1}$$

$\text{Tr}_R(*)$ is the partial trace over the reset qubit and $\rho_R = \frac{1}{e^{-\epsilon}+e^{\epsilon}} \begin{pmatrix} e^{\epsilon} & 0 \\ 0 & e^{-\epsilon} \end{pmatrix}$, is the fixed point of the reset process. The parameter ϵ is called the polarization and $\epsilon = \frac{\Delta}{2K_bT_B}$, where Δ is the energy gap of the reset qubit, K_b is the Boltzmann constant, and T_B is the temperature of the heat-bath. Polarization is commonly used to quantify the purity of spins. The higher the polarization, the purer and colder the qubit is. For a qubit with the state $\rho = \begin{pmatrix} a & 0 \\ 0 & b \end{pmatrix}$ the polarization is given by $\frac{1}{2} \log \left(\frac{a}{b} \right)$.

We use $[\rho^t] = \left\{ \lambda_1^{(t)}, \lambda_2^{(t)}, \cdots \lambda_{2^{n+1}}^{(t)} \right\}$ to show the state of n computation qubits plus one reset qubit which is the last one. The superscript represents the iteration index and the subscript is the index of the diagonal elements.

The state after the reset is $[\rho^{\infty}] = \left\{ p_0^{\infty}, p_1^{\infty}, \cdots p_{2^n-1}^{\infty} \right\} \otimes [\rho_R]$, where the first part represents the state of the n computation qubits. The reset step cools down the reset qubit and changes the diagonal elements of the density matrix which also changes their ordering. For instance, for some specific i, it could be that $p_i e^{-\epsilon} \leq p_{i+1} e^{\epsilon}$.

After the reset, the sort operation in the following iteration would then increase the polarization of computation qubits. Figure 4.2 shows the procedure of each iteration.

4.3 Asymptotic state of HBAC

HBAC cools the first qubit monotonically which means that we just need to find the asymptotic temperature to find the cooling limit. If the system converges to an asymptotic state (which we show happens), then this state determines the cooling limit.

4.3.1 Steady state condition

Despite the simplicity of each iteration, the dynamics are complicated and it is difficult to understand how the state evolves under these dynamics. In particular, even assuming the system converges to an asymptotic state, it is challenging to find the asymptotic state
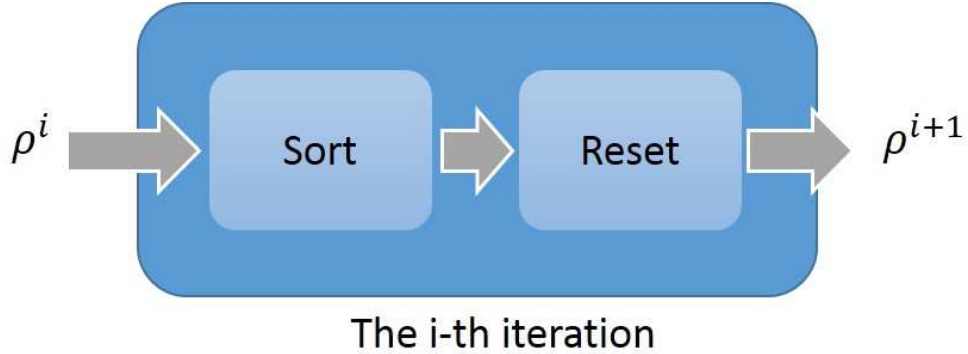
Figure 4.2: The schematics of each iteration of PPA algorithmic cooling. The diagonal elements of the density matrix are sorted decreasingly and the sort increases the polarization of the first computation qubit and decreases the polarization of the reset qubit. Next the reset process, refreshes the reset qubit and restores its initial polarization.

[55, 53]. Note that the sort operation depends on the probability distribution and thus is changing in each iteration. Thus results for time-homogeneous Markov processes (such as conditions under which they converge to a steady state) do not apply to the cooling process.

We use the fact that an asymptotic state should be invariant under PPA and first identify steady states of the PPA. This gives a necessary condition for the asymptotic state. We then specify the asymptotic state by proving a condition on the dynamics of PPA.

The asymptotic state does not change under the operations of HBAC and is a fixed point of the dynamics. Technically this implies that if it is reset, it still will be sorted. We mentioned that the state after the reset is $[\rho^\infty] = \left\{ p_0^\infty, p_1^\infty, \cdots p_{2^n-1}^\infty \right\} \otimes [\rho_R]$,.

The fact that the full density matrix is sorted after the reset step, implies that $p_i^\infty e^{-\epsilon} \geq p_{i+1}^\infty e^{\epsilon}$, $\forall i$.

Note that this condition does not specify the asymptotic state. In fact the steady state is not unique and any state that satisfies the condition above is invariant under PPA. Therefore the invariance under PPA is a necessary condition, but not sufficient. This was also recognized in [53] where the state in Equation (4.5) was found and shown to establish a lower bound on the asymptotic polarization. Their numerical evidence [53], and other numerical studies independent of this work [145], suggested the bound is tight when the initial state is maximally mixed.

4.3.2 Evolution condition

One of the key elements of our work is the following theorem which specifies the steady state that is the asymptotic state of HBAC. It states that while the distances between consecutive p_i are increasing in PPA, the ratio of two consecutive diagonal elements of the density matrix would never exceed $e^{2\epsilon}$.

For simplicity we define a distance. Consider two consecutive elements of the density matrix, p_i and p_{i+1}. We define the following distance between the elements of the density matrix

$$d_i \overset{\text{Def}}{=} \log \frac{p_i}{p_{i+1}}. \tag{4.2}$$

Theorem 1. *For PPA algorithmic cooling with a reset qubit $[\rho_R] = \frac{1}{e^{-\epsilon}+e^{\epsilon}}\{e^{\epsilon}, e^{-\epsilon}\}$, for any iteration t and $i, 0 \leq i \leq 2^n - 1$, $\frac{p_i^t}{p_{i+1}^t} \leq \max\left\{e^{2\epsilon}, \frac{p_i^0}{p_{i+1}^0}\right\}.$*

The sketch of the proof is as follows. For any index i and any iteration t, if the ratio of $\frac{p_i^t}{p_{i+1}^t} \leq e^{2\epsilon}$, then we can show that $p_i^{t+1} \leq e^{\epsilon}\left(p_i^t + p_{i+1}^t\right)$ and $p_{i+1}^{t+1} \geq e^{-\epsilon}\left(p_i^t + p_{i+1}^t\right)$ and as a result $\frac{p_i^{t+1}}{p_{i+1}^{t+1}} \leq e^{2\epsilon}$. On the other hand, if the ratio of $\frac{p_i^t}{p_{i+1}^t} \geq e^{2\epsilon}$, then it is easy to see that $\frac{p_i^{t+1}}{p_{i+1}^{t+1}} \leq \frac{p_i^t}{p_{i+1}^t}$. Note that the sort operation in this case could only decrease p_i or increase p_{i+1}, both of which leads to a lower $\frac{p_i^{t+1}}{p_{i+1}^{t+1}}$. Therefore we can always bound $\frac{p_i^{t+1}}{p_{i+1}^{t+1}} \leq \max\left\{e^{2\epsilon}, \frac{p_i^t}{p_{i+1}^t}\right\}$. Induction on t completes the proof of the theorem. A more detailed proof is given in the 4.7.

If the initial state satisfies $d_i^0 \leq 2\epsilon$ for all i, which holds, for a broad class of states like the maximally mixed state or the thermal state when the computation qubits have a smaller gap than the reset qubit, then one obtains the following condition for the asymptotic state:

$$p_i^{\infty} e^{-\epsilon} = p_{i+1}^{\infty} e^{\epsilon}, \forall i, \tag{4.3}$$

where p_i are the diagonal elements of the density matrix of computation qubits. Note that in general, it could be that $d_i^0 \geq 2\epsilon$. We investigate the more general case in 4.7.

4.3.3 Asymptotic state

The condition in Eq. (4.3) together with the normalization of the state is enough to determine the full state. Equation (4.3) can be rewritten as $p_i^{\infty} = e^{-2i\epsilon} p_0^{\infty}$ and considering

The comparison between the upperbound and λ_1^∞

— The Upperbound
— Actual λ_1^∞
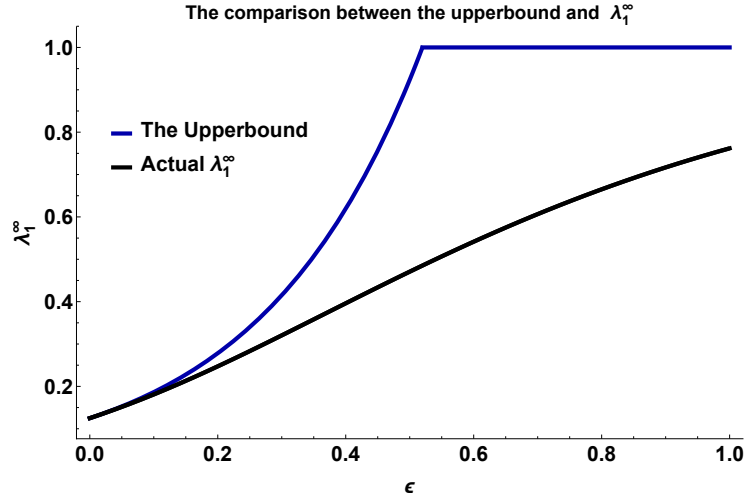
Figure 4.3: Comparison of the upper bound and value of λ_1^∞. The gap between the upper bound and the actual value gets larger as ϵ, the polarization of the reset qubit increases.

state normalization gives:

$$p_0^\infty = \frac{e^{-2\epsilon} - 1}{\left(e^{-2\epsilon}\right)^{2^n} - 1}. \tag{4.4}$$

Comparison with previous results

Schulman et al. upper bounded λ_1^∞ by $\frac{e^{2^n\epsilon}}{2^n}$ in [153] which is consistent with our result. Note that $\lambda_1^\infty = \frac{e^\epsilon}{e^{-\epsilon}+e^{-\epsilon}}p_0^\infty$. Figure 4.3 gives a comparison between this bound and the actual value from equation (4.4). Plots are for $n = 2$ and one reset qubit. Figure 4.3 illustrates how the upper bound in [153] compares to the actual value.

Asymptotic state and temperature

Equations (4.3) and (4.4) give the asymptotic state

$$[\rho^\infty] = p_0^\infty \left\{1,\, e^{-2\epsilon},\, e^{-4i\epsilon},\, \cdots\right\} \otimes \rho_R. \tag{4.5}$$

The first qubit has the lowest temperature. Therefore, we focus on the first computation qubit for finding the cooling limit. We find that the polarization of the first qubit is

$$P = 2^{n-1}\epsilon. \tag{4.6}$$

34
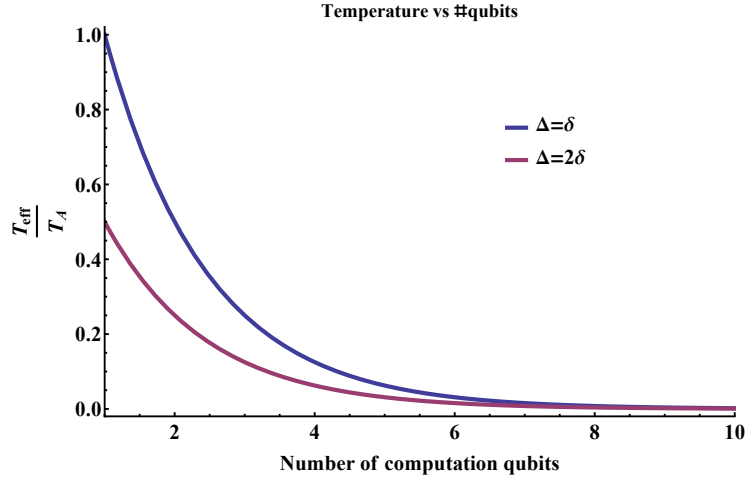
Figure 4.4: Asymptotic cooling ratio. The cooling limit depends on the number of qubits and the ratio of the energy gaps of the computation qubit to the one for the reset qubit, $\frac{\delta}{\Delta}$. The cooling limit improves exponentially with increasing n and linearly with decreasing $\frac{\delta}{\Delta}$.

This result is consistent with the lower bound that was calculated in [53], in the case of $\epsilon \ll \frac{1}{2^n}$. In fact we proved that this lower-bound is tight.

Equation (4.6) shows that the performance of HBAC increases exponentially with the number of qubits, n. The simple way to see this is to look at the effective temperature. The effective temperature of the first qubit is

$$T_{\text{eff}} = \frac{\delta}{\Delta} \frac{T_B}{2^{n-1}}, \tag{4.7}$$

where δ is the energy gap of the qubit and is often different from Δ, the energy gap of the reset qubit. Usually the reset and computation qubits should be of different species as the reset qubits have a shorter relaxation time. The cooling limit would improve if the energy gap of the reset qubit is much larger than the one for the computation qubits. For instance, if an electron is used as the reset qubit and hydrogen nuclear spins for computation, this ratio would be $\frac{1}{660}$ which lowers the cooling limit by a factor of 660.

Figure 4.4 shows how the effective temperature decreases with increasing the number of computation qubits, n. It also shows that changing the $\frac{\delta}{\Delta}$ changes the cooling limit.

4.3.4 Generalization of the reset process

We can also answer one of the important questions about HBAC, namely, identifying how the performance of HBAC depends on the energy spectrum of the reset system in the case of higher dimensional reset systems.

Equation (4.3) can be generalized for arbitrary reset state, ρ_R. For a D-level reset system we get a similar condition as in equation (4.3) with the difference that the gap is replaced by the sum of the gaps. We refer to this as the "large gap" and use Δ_{total} to show it. The cooling limit for qudits is

$$T_{\text{eff}} = \frac{\delta}{\Delta_{total}} \frac{T_B}{2^{n-1}}, \tag{4.8}$$

which similar to the one in Equation (4.7) with Δ replaced by Δ_{total}.

It is interesting that despite the more complicated energy structure of the reset qubit, the "large gap" is the only parameter that would influence the cooling limit. In particular, the cooling limit does not directly depend on the number of energy levels or the spacing between them, as long as the total gap does not change.

Multi-qubit Reset

This result also has an interesting implication for multi-qubit reset systems. The energy gap of a multi-qubit reset system is the sum of the energy gaps of the individual qubits. As a result the large gap increases as one adds reset qubits, and this improves the cooling limit. For instance, if k identical qubits are used for the reset, then the energy gap would be $\Delta_{total} = k\,\Delta$ and it lowers the cooling limit by a factor of $\frac{1}{k}$. In other words, using such a multi-qubit reset is linearly better (in terms of the number of qubits) than using a single qubit reset.

Note that the energy structure of the reset system could still change the complexity or the number of operations for HBAC but the asymptotic state only depends on the largest gap of the reset system.

4.4 Decoherence

So far, we have studied PPA algorithmic cooling under the assumption of perfect operation and no decoherence. In practice however, there are imperfections in the implementation.

These experimental imperfections could affect the minimum achievable cooling. The HBAC operations are optimized based on the probability distribution at each step, and thus unknown errors in the probability distribution mean the cooling steps will not be optimal.

It is therefore critical to investigate these imperfections. Some of these, like decoherence has been recently studied [22].

Note that it is unclear if it is possible to go around these imperfections with fault tolerance. This is because fault tolerance requires ancillary qubits with high purity and the main purpose of HBAC is to provide these ancillary qubits. So assuming that we can do the operations of HBAC with fault tolerance is not practical.

HBAC techniques are often quite complicated even in the absence of the imperfections. In most cases, it is not clear how different noise processes would affect the implementation and final outcome of the HBAC. In principle, some imperfections may even improve the asymptotic limit of cooling.

An obvious noise model that reduces the asymptotic cooling, is a coherent noise model where every operation is conjugated by some unitary which may even change from one iteration to the other. Imperfections in the control could lead to these kind of noise. For instance, a x-rotation by θ may be implemented with some deviation which gives $R_x(\delta\theta)R_x(\theta)$. Consider PPA where the operations are permutations. It is shown that if permutations are followed by some unitary, the final density matrix would have a higher temperature than the state of the perfect PPA [153].

On the other hand, one can in principle imagine some imperfection that improves the cooling limit of HBAC. For instance, consider the following noise model

$$U\rho U^\dagger \to C(\rho) = (1-p)U\rho U^\dagger + p|0\rangle\langle 0|. \tag{4.9}$$

Although this may not be a realistic noise model, it shows that noise may in principle improve HBAC.

4.5 Complexity of the Implementation

On of the critical problem about the HBAC is the implementation costs. This is often analysed in terms of the number of iterations required [154, 153, 145]. However the number of operations is not necessary a good cost function.

In particular for PPA algorithmic cooling, the implementation cost of each iteration may be exponential in n, which means that although the total number of operations to achieve a certain polarization may be polynomial in n, the total cost may still be exponential.

PPA is one of the most challenging HBAC techniques from the implementation point of view. This is mainly because of two reasons:

1. Permutations are changing from one iteration to the other.

2. Each iteration involves implementing a unitary over n qubits and it is not clear that there is an efficient way to implement the permutation.

Further investigation is required to show that PPA is efficiently implementable as well as to address how to implement it.

4.6   Conclusion and Applications

In conclusion, we establish the fundamental limit of cooling for all HBAC techniques and show that it reduces exponentially with the number of qubits. It also depends on the ratio of the energy gap of the reset qubit to the gap of the computation qubits. We studied the effects of the changes to the energy spectrum of the reset system and showed that only the large gap of the reset system affects the asymptotic state. In particular, the number of energy levels, for a constant energy gap, does not influence the cooling limit.

Note that this limit is different from the third law of thermodynamics [117, 111]. With HBAC the temperature does not approach zero as time or the number of iterations approaches infinity.

Note that experimental imperfections could affect the minimum achievable cooling. The HBAC operations are optimized based on the probability distribution at each step, and thus unknown errors in the probability distribution mean the cooling steps will not be optimal. It is therefore critical to investigate these imperfections. Some of these, like depolarization, have been recently studied [22].

Besides the fundamental significance, the cooling limit could have practical applications as well. For instance, it could give a quantitative measure of imperfection for implementing and studying the HBAC. One natural choice would be the distance from the asymptotic state, ρ^∞, which requires the full density matrix. This may be expensive experimentally.

An easier solution is $|p_0 - p_0^\infty|$ which approaches zero as the state approaches the asymptotic cooling limit. Or, simply $|P_0 - 2^{n-1}\epsilon|$, where P_0 is the achieved polarization of the first computation qubit.

For experimental implementation of HBAC, this measure quantifies how far the experiment is from the cooling limit and gives a metric for the assessment of the progress in the experiment.

Similarly, it can be used for theoretical cost analysis of HBAC which requires a notion of distance from the asymptotic state. The number of operations that are needed to achieve a certain fidelity to the asymptotic state can be calculated in terms of such a distance. Some studies have investigated this problem in terms of the number of iterations required [154, 153, 145]. By calculating the cost of an iteration in terms of resources such as gates, time or energy, one could build on these works in order to calculate the resource cost of implementing HBAC, and to decide when the costs of additional iterations of HBAC no longer outweigh the benefits of further cooling.

4.7   Proofs

We first prove the Theorem (1) in the paper and its extension for qudit reset and then prove the convergence of the PPA algorithmic cooling.

Before we get to the proof, it is useful to explain a few details about the dynamics and the update rules of the PPA.

We start by explaining "crossings" which are the building block of the cooling in PPA.

Crossings

When the reset qubit is reset, the ordering of the elements on the diagonal of the density matrix changes. These changes are what lead to the cooling. The reset step takes the state $[\rho] = \{\lambda_1, \lambda_2, \cdots \lambda_{2^{n+1}}\}$ of n computation qubits and one reset qubit to

$$\left[\rho'\right] = \{p_0, p_1, \cdots p_{2^n-1}\} \otimes [\rho_R],$$

where $p_i = \lambda_{2i+1} + \lambda_{2i+2}$ and $[\rho_R] = \{e^\epsilon, e^{-\epsilon}\}/z$. This can be generalized for the reset with a qudit $[\rho_R] = \{a_1, a_2, ..., a_k\}$ as well. For convenience, we assume these values are

sorted (so $a_1 \geq a_2 \geq \ldots \geq a_k$) [1]. Although the probabilities p_i are sorted, the full density matrix is not necessarily sorted. For instance, for some indices $i < j$, and $m_i > m_j$, we could have

$$p_i a_{m_i} < p_j a_{m_j}, \tag{4.10}$$

In this case, the sort operation in PPA would rearrange the terms and update the value of p_i. We refer to this condition as "crossing from below" for the ith probability. Similar crossing for the ith probability could occur from above which we refer to as "crossing from above".

Despite the complexity of different crossings, we can make the following general remarks.

Remark 2. **Crossing from above** If p_i combined with the reset qudit probabilities gives the values $\{p_i a_1, p_i a_2, \cdots p_i a_k\}$ and there is crossing from above (and none from below), the sort operation on all $k2^n$ probabilities yields the values $\lambda_1 \geq \lambda_2 \geq \cdots \geq \lambda_k = p_i a_k$ for the $(ik+1)$th, $(ik+2)$th, $\ldots (ik+k)$th probabilities (i.e. the probabilities that will add up to determine p_i') such that

$$p_i a_j \geq \lambda_j \geq p_i a_k. \tag{4.11}$$

Proof. The second inequality is easier to see. It comes from the fact that $\forall j < i$, $p_j \geq p_i$ and therefore, for any m, we have $p_j a_m \geq p_i a_k$.

The first inequality comes from the ordering. The value λ_j is by definition the first element that is $\geq \lambda_{j+1}$. One can use induction (starting with $k = j + 1$ as the base case) to prove the first inequality. Specifically, if $\lambda_{j+1} \leq p_i a_{j+1}$ then (since $a_j \geq a_{j+1}$) we have $p_i a_j \geq \lambda_{j+1}$ implies which implies that $\lambda_j \leq p_i a_j$.

$\square$

Remark 3. **Crossing from below** If p_{i+1} combined with the reset qudit probabilities gives the values $\{p_{i+1} a_1, p_{i+1} a_2, \cdots p_{i+1} a_k\}$ and there is crossing from below (and none from above), the sort operation on all $k2^n$ probabilities yields the values $\delta_1 = p_{i+1} a_1 \geq \delta_2 \geq \cdots \geq \delta_k$ for the $((i+1)k+1)$th, $((i+1)k+2)$th, $\ldots ((i+1)k+k)$th probabilities such that

$$p_{i+1} a_j \leq \delta_j \leq p_{i+1} a_1. \tag{4.12}$$

---

[1] Depending on the physical system, one might simply label the states in this way. For other physical systems, the natural labelling might not be in descending order of probability. In these cases, one must account for this labelling when computing the permutation of the combined computational and reset system. For example, for a reset qudit that is the product of identical qubits, the reset system probabilities will not follow a lexicographic ordering. The probabilities will decrease as the Hamming weight of the strings increase. The appropriate permutation of these reset system strings (or alternatively, the corresponding conjugation of the permutation of the combined system) will affect the overall complexity of implementing the HBAC permutations.

The proof is similar to the one for crossing from above.

We use the distance and generalise the Theorem (1) in the following way.

Theorem 4. *For PPA algorithmic cooling with a reset qudit $[\rho_R] = \{a_1, a_2, ..., a_k\}$ where a_l are sorted decreasing and sum to 1 and for any iteration t , $d_i^t \leq \max\left\{d_i^0, \log\frac{a_1}{a_k}\right\}$.*

Proof. We focus on d_i for some arbitrary iteration and prove the bound.

After the reset step of the iteration, we break down the sort operation into two steps. First we separately sort the values $p_u a_l$ for $u \geq i+1$, and also the values $p_v a_l$ for $v \leq i$. This means that the sort does not involve sorting between terms of the form $p_i a_l$ and $p_{u \geq i+1} a_l$ nor between terms of the form $p_{i+1} a_l$ and $p_{v \leq i} a_l$.

Let λ_j be the $(k - j + 1)$th smallest number after the sort operation among the $p_j a_l$ values for $j \leq i$ and let δ_j be the jth largest value after the sort operation among the $p_j a_l$ values for $j \geq i + 1$. Note that $\delta_1 = p_{i+1} a_1$ and $\lambda_k = p_i a_k$. In the next step we complete the sort by combining and sorting the probabilities that lie between $p_{i+1} a_1$ and $p_i a_k$.

Let's first consider the case that $\lambda_1 \geq \delta_1$ and $\lambda_k \geq \delta_k$. Then when we merge and resort the λ_j and δ_j values, for some integer $r \geq 0$ the values $\delta_1, \delta_2, \ldots, \delta_r$ will appear among the largest k values, and $\delta_{r+1}, \ldots, \delta_k$ will appear among the smallest k values. Similarly, the values $\lambda_1, \ldots, \lambda_{k-r}$ will appear among the largest k values, and the values $\lambda_{k-r+1}, \ldots, \lambda_k$ will appear among the smallest k values.

The sub-case where $r = 0$ corresponds to when there is no crossing between p_i and p_{i+1} (i.e. $p_i a_k \geq p_{i+1} a_1$) and we will come back to this case as well.

Let us next consider the sub-case that $1 \leq r \leq k/2$. Thus we get

$$p_i' = \sum_{j=1}^{r} (\lambda_j + \delta_j) + \sum_{j=r+1}^{k-r} \lambda_j$$

$$p_{i+1}' = \sum_{j=k-r+1}^{k} (\lambda_j + \delta_j) + \sum_{j=r+1}^{k-r} \delta_j.$$

41

Using Remark 2 and Remark 3 we find the following bounds

$$p'_i \leq \sum_{j=1}^{r} (p_i a_j + p_{i+1} a_1)$$

$$+ \sum_{j=r+1}^{k-r} p_i a_j \leq r a_1 (p_i + p_{i+1}) + p_i \chi$$

$$p'_{i+1} \geq \sum_{j=k-r+1}^{k} (p_i a_k + p_{i+1} a_j)$$

$$+ \sum_{j=r+1}^{k-r} p_{i+1} a_j \geq r a_k (p_i + p_{i+1}) + p_{i+1} \chi,$$

where $\chi = \sum_{j=r+1}^{k-r} a_j$. We want to show that $\frac{p'_i}{p'_{i+1}} \leq \frac{a_1}{a_k}$ which follows from the fact that $p_i a_k \leq p_{i+1} a_1$ when there is at least one crossing between p_i and p_{i+1}. In other words,

$$\frac{p'_i}{p'_{i+1}} \leq \frac{r a_1 (p_i + p_{i+1}) + p_i \chi}{r a_k (p_i + p_{i+1}) + p_{i+1} \chi} \leq \frac{r a_1 (p_i + p_{i+1})}{r a_k (p_i + p_{i+1})} \leq \frac{a_1}{a_k}.$$

Let us next consider the sub-case that $k/2 < r < k$. Thus we get

$$\Rightarrow p'_i = \sum_{j=1}^{k-r} (\lambda_j + \delta_j) + \sum_{j=k-r+1}^{r} \delta_j$$

$$\Rightarrow p'_{i+1} = \sum_{j=r+1}^{k} (\lambda_j + \delta_j) + \sum_{j=k-r+1}^{r} \lambda_j.$$

Using Remark 2 and Remark 3 we find the following bounds

$$p'_i \leq (k-r)(p_i + p_{i+1})a_1 + (2r - k)p_{i+1}a_1$$
$$p'_{i+1} \geq (k-r)(p_i + p_{i+1})a_k + (2r - k)p_i a_k$$
$$\Rightarrow p'_i / p'_{i+1} \leq \frac{((k-r)(p_i + p_{i+1}) + (2r-k)p_{i+1}) a_1}{((k-r)(p_i + p_{i+1}) + (2r-k)p_i) a_k}$$
$$\leq \frac{((k-r)(p_i + p_{i+1}) + (2r-k)p_{i+1}) a_1}{((k-r)(p_i + p_{i+1}) + (2r-k)p_{i+1}) a_k} \leq \frac{a_1}{a_k}.$$

For the case where $r = 0$, we get

$$p'_i = \sum_{j=1}^{k} \lambda_j \leq \sum_{j=1}^{k} p_i a_j = p_i$$

$$p'_{i+1} = \sum_{j=1}^{k} \delta_j \geq \sum_{j=1}^{k} p_{i+1} a_j = p_{i+1}.$$

It follows that $\frac{p'_i}{p'_{i+1}} \leq \frac{p_i}{p_{i+1}}$.

Now we get to the case when either all the $\lambda_j \leq \delta_1 = p_{i+1} a_1$ or when all the $\delta_j \geq \lambda_k = p_i a_k$ (or both). If it is the former, we get $p'_i \leq k\delta_1 = kp_{i+1} a_1$ and we also know that $p'_{i+1} \geq kp_{i+1} a_k$ which gives the desired result. Similarly, if all the $\delta_j \geq \lambda_k$ then $p'_{i+1} \geq k\lambda_k = kp_i a_k$ and $p'_i \leq kp_i a_1$ which again leads to $p'_i/p'_{i+1} \leq a_1/a_k$.

So the distance d'_i is bounded above by $\max\left\{d_i, \log\frac{a_1}{a_k}\right\}$ which proves the theorem.

$\square$

Note that for the case of $k = 2$ and $a_1 = e^\epsilon$ and $a_2 = e^{-\epsilon}$ we get Theorem (1).

Now we use this to prove that all of the p_i converge.

To prove the convergence, we first prove that p_0 converges and then the convergence of all the p_i follows from that. In order to make the connection between the convergence of p_0 and other p_i, we use Theorem 4.

Theorem 5. *Let p_0^t be the first diagonal element of the reduced density matrix of the computation qubits in the tth iteration of PPA algorithmic cooling. Then $\lim_{t\to\infty} p_0^t = p_0^\infty$, for some constant p_0^∞.*

Proof. The sequence of values p_0^t are increasing because there can only be crossings from below for p_0. The sequence is also upper-bounded, therefore it must converge: $p_0^\infty = \lim_{t\to\infty} p_0^t$. $\square$

Theorem 6. *Let p_i^t be the ith diagonal element of the reduced density matrix of the computation qubits in the tth iteration of PPA algorithmic cooling with a qubit reset $[\rho_R] = \frac{1}{e^{-\epsilon}+e^\epsilon}\{e^\epsilon, e^{-\epsilon}\}$. Then assuming that $d_i^0 \leq 2\epsilon, \forall i$, the limit $\lim_{t\to\infty} p_i^t = e^{-2i\epsilon} p_0^\infty$ exists. We refer to the limit as p_i^∞.*

Proof. We already proved that the p_0^∞ exists. This means that

$$\lim_{t \to \infty} (p_0^{t+1} - p_0^t) = 0. \tag{4.13}$$

On the other hand, as $p_0^{t+1} = p_0^t \frac{e^\epsilon}{z} + p_1^t \frac{e^\epsilon}{z}$ we find that 4 implies that as $t \to \infty$

$$p_0^{t+1} - p_0^t = p_1^t \frac{e^\epsilon}{z} - p_0^t \frac{e^{-\epsilon}}{z}. \tag{4.14}$$

The limit of the last term, $p_0^t \frac{e^{-\epsilon}}{z}$ exists and the left hand side converges to zero, so $\lim_{j \to \infty} p_1^t$ must be $e^{-2\epsilon} p_0^\infty$. The convergence of the rest of the p_i^t follows by induction. Note that although there could be crossings from above for $i \geq 1$, the change from above approaches zero and we get

$$p_i^{t+1} - p_i^t = \zeta_i^t + p_{i+1}^t \frac{e^\epsilon}{z} - p_i^t \frac{e^{-\epsilon}}{z}, \tag{4.15}$$

where ζ_i^t corresponds to the change to p_i due to crossing from above, where for sufficiently large t (once the p_j^t, for $j \leq i$, are close enough to p_j^∞ that there is at most one crossover between p_j^t and p_{j-1}^t), we have $\zeta_i^t = (p_{i-1}^t e^{-\epsilon} - p_i^t e^\epsilon)/z$.

Since (for sufficiently large t) $p_{i-1}^{t+1} - p_{i-1}^t = (p_{i-2}^t e^{-\epsilon} - p_{i-1}^t e^\epsilon)/z + (p_i^t e^\epsilon - p_{i-1}^t e^{-\epsilon})/z = p_{i-2}^t e^{-\epsilon}/z - p_{i-1}^t e^\epsilon/z - \zeta_i^t$, then taking $lim_{t\to\infty}$ of both sides yields

$$\lim_{t \to \infty} \zeta_i^t = 0.$$

Therefore we get

$$p_{i+1}^\infty = e^{-2\epsilon} p_i^\infty. \tag{4.16}$$

$\square$

For the PPA with a reset qudit $[\rho_R] = \{a_1, a_2, ..., a_k\}$, the proof is similar. As $j \to \infty$ we get $(p_0^{t+1} - p_0^t) - (p_1^t a_1 - p_0^t a_k) \to 0$ and since as $t \to \infty$ the left hand side and the last term converge, so does p_1^t. The rest of the proof follows similarly.

If we start with a maximally mixed state for the computation qubits, $d_i^0 = 0$, i.e. initially all the distances are zero, then for any iteration t and any index i, we get

$$d_i^t \leq \log\left(\frac{a_1}{a_k}\right) \tag{4.17}$$

and thus Theorem 6 (and its generalization to qudits) applies.

44

Note that for the case where the qubits are not initially in the maximally mixed state, Theorem 4 still applies and can be used to find the asymptotic state. A sufficient condition for getting the asymptotic state in Equation (4) is that $\log_2(\frac{p_0^0}{p_{2^n-1}^0}) \leq 2(2^n - 1)\epsilon$.

For the more general case of $[\rho^0] = \{p_0^0, p_1^0, \ldots, p_{2^n-1}^0\}$, it is more complicated to determine the asymptotic state, however, Theorem 4 applies. In this case, the probabilities could be grouped in different blocks of consecutive probabilities where in each block, the distance between any two consecutive p_i^0 is less than 2ϵ and is greater between two different blocks. These blocks are referred to as assemblies [33]. Using theorem 4 , we can see that the distance between the probabilities in each assembly would increase to 2ϵ. This also implies that two neighbouring assemblies may merge together. To find the asymptotic state, we can go through the expansion and merger of all the assemblies until the final asymptotic state is found. The asymptotic state would be a combination of different assemblies (referred to maximal assemblies in [33]) where $d_i = 2\epsilon$ inside the blocks and is $d_i > 2\epsilon$ in between the assemblies.

Chapter 5

Quantum information approach to Bose-Einstein condensation of composite bosons

Most of the content of this chapter was published in [108]. I contributed to the main ideas and the calculations in this work. Specifically, I did some of the calculations, double checked the rest of them and produced some of the plots.

5.1 Introduction

The idea of Bose-Einstein condensation (BEC) was originally introduced for a uniform, non-interacting gas of elementary bosons [75]. In reality, BEC experiments are conducted using potential traps for gases of bosonic particles, like alkali atoms, atomic hydrogen or metastable helium, that are composite particles made of fermions, and for which inter-particle interactions cannot be neglected [2, 18, 44]. Alternative BEC scenarios also take into account composite systems, e.g., condensation of fermionic pairs in liquid ^{3}He [134] or excitons (electron-hole pairs) in bulk semiconductors [16, 41, 52, 88]. In addition, these BEC scenarios are closely related to other macroscopic quantum phenomena like superfluidity and superconductivity [133].

In many studies the internal structure of composite particles is neglected. On the other hand, it was noted that in some cases this structure plays an important role [146, 149, 39, 36, 40, 38]. Therefore, it is interesting to see how BEC can be affected by the

internal structure of composite bosonic particles. Previously BEC was investigated with the interpolation between bosonic and fermionic statistics [6], and with individual exchanges between the constituent fermions [37].

In this work we consider a simple model of BEC with composite bosonic particles. In particular, we assume that neither the composite particles nor their constituents interact, such that the internal structure of composite particles is stable and temperature independent.

Of course, the bound states between constituent particles have to result from their interaction. However, here we assume that once the constituents form a composite particle state, they do not interact anymore. Physically, this may correspond to a dilute gas of composite particles for which energy scales of a binding interaction potential between constituents are much greater than energy scales of the confining trap. As an example, one may think of an atomic hydrogen gas in which ionization temperature is much higher than the standard temperatures required to obtain BEC. Such a simplified model allows us to focus on the fundamental problem of how BEC depends on the internal state of composite particles, while neglecting other physical properties.

Nowadays, the phenomenology of composite bosons such as excitons, can be explained using the tools developed by quantum information theory [38]. The role of quantum correlations between constituents forming a bound composite particle state can be studied qualitatively and quantitatively using the notion of entanglement. In particular, it was shown that the degree of entanglement between a pair of fermions (bosons) is responsible for their behavior as a single bosonic particle, i.e., only entangled particles behave like a single boson and the more entanglement between them, the more (less) bosonic they are [105]. Here, we raise the question: how is BEC affected by the entanglement between the two constituent fermions or bosons?

5.1.1 Composite Bosons

Definition

Before we start our discussion, let us recall the important results that are relevant to this work. Imagine a pair of distinguishable fermionic or bosonic particles. The system is described by the creation operators $\hat{a}_k^\dagger$ and $\hat{b}_l^\dagger$, where the indices $k, l = 0, 1, \ldots, \infty$ label different modes that can be occupied by the two particles. These modes can for example correspond to different energies, or different momentum states. The wave function of the

system is of the form

$$\sum_{k,l=0}^{\infty} \alpha_{k,l} \hat{a}_k^\dagger \hat{b}_l^\dagger |0\rangle, \tag{5.1}$$

where $\alpha_{k,l}$ is the probability amplitude that particle a is in mode k and particle b is in mode l, and $|0\rangle$ is the vacuum state. Using insights from entanglement theory, the mathematical procedure known as the Schmidt decomposition allows us to rewrite the above state as [105]

$$\sum_{m=0}^{\infty} \sqrt{\lambda_m} \hat{a}_m^\dagger \hat{b}_m^\dagger |0\rangle \equiv \hat{c}^\dagger |0\rangle, \tag{5.2}$$

where the modes labeled by m are superpositions of the previous modes k and l and $\sqrt{\lambda_m}$ are probability amplitudes that both particles occupy mode m. Note that despite the fact that $\hat{a}_m^\dagger$ and $\hat{b}_m^\dagger$ share the same label, physically these modes might be totally different. What is important is that, the modes labeled by m give rise to the internal structure of a composite particle.

Entanglement of Composite Bosons

We have introduced a composite boson creation operator $\hat{c}^\dagger$, that creates a pair of particles. Note that this operator resembles the one for Cooper pairs [38]. The entanglement between particles is encoded in the amplitudes $\sqrt{\lambda_m}$. In particular, one can introduce a measure of entanglement known as *purity*

$$P = \sum_{m=0}^{\infty} \lambda_m^2, \quad 0 < P \le 1. \tag{5.3}$$

For $P = 1$ the particles are disentangled, whereas in the limit $P \to 0$ the entanglement between particles goes to infinity. The degree of entanglement can be also expressed via the so called Schmidt number $K = 1/P$. Intuitively, K estimates the average number of modes that are taken into account in the internal structure of a composite boson.

The bosonic properties of $\hat{c}^\dagger$ can be studied in many ways. For example, the commutation relation gives $[\hat{c}, \hat{c}^\dagger] = 1 + \xi \sum \lambda_m (\hat{a}_m^\dagger \hat{a}_m + \hat{b}_m^\dagger \hat{b}_m)$, where $\xi = -1$ if a and b are fermions, or $\xi = +1$ if they are bosons. On the other hand, following the approach in [105] one may

study the ladder properties of this operator

$$|n\rangle \equiv \chi_n^{-1/2} \frac{(\hat{c}^\dagger)^n}{\sqrt{n!}} |0\rangle,$$

$$\hat{c}|n\rangle = \sqrt{\frac{\chi_n}{\chi_{n-1}}} \sqrt{n} |n-1\rangle + |\epsilon_n\rangle, \ \langle n-1|\epsilon_n\rangle = 0, \quad (5.4)$$

$$\langle \epsilon_n|\epsilon_n\rangle = 1 - n \frac{\chi_n}{\chi_{n-1}} + (n-1) \frac{\chi_{n+1}}{\chi_n},$$

where $|n\rangle$ are states of n composite bosons, parameters χ_n are normalization factors, such that $\langle n|n\rangle = 1$, and $|\epsilon_n\rangle$ are unnormalized states that can result form subtracting a single composite particle from a state $|n\rangle$. The states $|\epsilon_n\rangle$ do not correspond to $n-1$ composite bosons of the same type, but rather to a complicated state of $n-1$ pairs of particles a and b. The ladder structure of operators $\hat{c}^\dagger$ and $\hat{c}$ starts to approach those of ideal bosons if $\frac{\chi_{n+1}}{\chi_n} \to 1$ for all n. In Ref. [105, 32] it has been shown that for a pair of fermions the ratio $\frac{\chi_{n+1}}{\chi_n}$ can be bounded from above and below by the function of entanglement

$$1 - nP \le \frac{\chi_{n+1}}{\chi_n} \le 1 - P.$$

Then, it has been improved with a tighter upper bound [174]

$$1 - nP \le \frac{\chi_{n+1}}{\chi_n} \le 1 - \frac{nP}{1 + (n-1)\sqrt{P}} \le 1 - P.$$

This result shows that in the limit of large entanglement ($P \ll 1/n$) the pairs of particles behave like real bosons. Other results on the relation between composite bosons and quantum correlations can be found in [174, 141, 176, 102, 175, 66, 65, 170, 173, 109, 31, 172].

To simplify our model, we assume BEC in Gaussian states which are represented by a combination of coherent, thermal, and squeezed states. Assuming that composite bosons are in a thermal state or in a harmonic trap, we can describe the composite bosons with a Gaussian state. Thus, the Gaussian formula of the composite bosons is represented by the following modified operator that is based on the one studied in [105]

$$\hat{c}_r^\dagger = \sum_{m=0}^{\infty} \sqrt{(1-x)x^m} \hat{a}_{m,r}^\dagger \hat{b}_{m,r}^\dagger, \quad (5.5)$$

where the double indices refer to internal (m) and to external degrees of freedom (r). The internal index m represents their position values when the proton and electron are

strongly correlated [32]. In our case r labels the energy levels of the trap in which the BEC takes place. Moreover, as we assumed in the beginning, the internal structure parameters $\lambda_m = (1 - x)x^m$ (for $0 \leq x < 1$) are independent of r. The above operator has desirable properties, since it is possible to analytically evaluate the factors χ_n and one can control the entanglement between constituents a and b via the parameter x [105]. For $x = 0$ the system is separable and in the limit $x \to 1$ entanglement goes to infinity. In addition

$$0 \leq (\frac{\chi_{n+1}}{\chi_n})_F = \frac{x^n(n + 1)(1 - x)}{(1 - x^{n+1})} < 1 \tag{5.6}$$

for a pair of fermions [105] and

$$1 < (\frac{\chi_{n+1}}{\chi_n})_B = \frac{(n + 1)(1 - x)}{(1 - x^{n+1})} \leq n + 1 \tag{5.7}$$

for a pair of bosons [105]. Finally, the Schmidt number is given by [105]

$$K = \frac{1 + x}{1 - x}. \tag{5.8}$$

The rest of the paper is organized as follows. We begin with investigating the meaning of $\langle \hat{c}_r^\dagger \hat{c}_r \rangle$. Then, we discuss the BEC of composite bosons made of fermionic pairs. We consider two cases, a potential trap with only two levels and the 3D harmonic potential trap with an infinite number of energy states. Next, we repeat the same for the composite bosons made of bosonic pairs. Finally, we analyze our results in the last section.

5.2 Number-operator mean value of cobosons

Before going ahead, we look into the meaning of the number-operator mean value (NMV) of cobosons. Using the Eqs. (4) and (5), we evaluate the NMV of cobosons in an N number state $|N\rangle_r$, which represents N cobosons on the r-th energy level,

$$_r\langle N|\hat{c}_r^\dagger \hat{c}_r|N\rangle_r = 1 + (N - 1)\frac{\chi_{N+1}}{\chi_N},$$

where $(\chi_{N+1}/\chi_N) = 1$ as the cobosons become ideal bosons. For pairs of fermions, the normalization ratio $(\chi_{N+1}/\chi_N)_F$ is less than one due to the Pauli exclusion principle between pairs fermions. Thus, $_r\langle N|\hat{c}_r^\dagger \hat{c}_r|N\rangle_r$ is less than the number of cobosons. We can imagine that the other cobosons move to other energy levels due to the Pauli exclusion
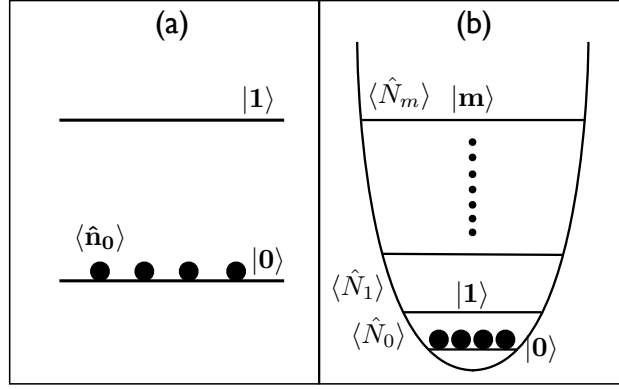
Figure 5.1: BEC using indistinguishable cobosons in (a) a two-level system and (b) a multi-level system.

principle. It requires that the number of cobosons be less than the number of energy levels. For pairs of bosons, the normalization ratio $(\chi_{N+1}/\chi_N)_B$ is larger than one due to the bunching effect between the two constituent bosons. Thus, $_r\langle N|\hat{c}_r^\dagger \hat{c}_r|N\rangle_r$ is larger than the number of cobosons. We can imagine that the extra cobosons came out of wave nature of the two constituent bosons. It is explained by the second-order correlation functions which represent intensity-intensity correlations [113], as below.

Expanding the Eq. (5) in the $_r\langle N|\hat{c}_r^\dagger \hat{c}_r|N\rangle_r$, the NMV of the cobosons is given by

$$_r\langle N|\hat{c}_r^\dagger \hat{c}_r|N\rangle_r = \sum_{n=m}^{\infty} \lambda_n \langle \hat{a}_{n,r}^\dagger \hat{a}_{n,r} \hat{b}_{n,r}^\dagger \hat{b}_{n,r}\rangle \qquad (5.9)$$
$$+ \sum_{n\neq m}^{\infty} \sqrt{\lambda_n \lambda_m} \langle \hat{a}_{n,r}^\dagger \hat{a}_{m,r} \hat{b}_{n,r}^\dagger \hat{b}_{m,r}\rangle.$$

The first term is the sum of unnormalized second-order correlation functions. The second term is, we called, the sum of cross correlation functions. According to the second-order correlation functions $G^{(2)}$[113], Gaussian states of bosons exhibit bunching effect with $1 < G^{(2)} < \infty$ whereas fermions exhibit anti-bunching effect with $0 \leq G^{(2)} < 1$. Based on the information of the $G^{(2)}$ functions, thus, we can understand the NMV of cobosons as follows. By bunching effect, pairs of bosons can produce large number rather than the number of cobosons. On the other hand, pairs of fermions can reduce the number of cobosons by anti-bunching effect, expelling the other cobosons to other energy levels.

Therefore, for pairs of fermions, we know that the NMV of cobosons can be same as a mean occupation number of cobosons in a multi-level system. For pairs of bosons, on the

other hand, the NMV of cobosons can be larger than the total mean occupation number of cobosons due to bunching effect between the two constituent bosons. In the next sections, we deal with the NMV of cobosons in a two-level system and a multi-level one.

5.3   BEC of Bi-Fermions

We consider indistinguishable cobosons in a two-level system and in a multi-level system, where each coboson is comprised of two fermions (bi-fermion). We investigate the case in which indistinguishable cobosons are in a Gaussian state, such that the normalization ratio of the coboson operator is represented by the parameter x [105]. From Eq. (8), x represents the degree of entanglement between a pair of fermions, where $x = 0$ ($x = 1$) means that a pair of fermions are separable (maximally entangled).

5.3.1   Two level approximation

First we consider a two-level system with a fixed number of N cobosons, see Fig. 1 (a). Although the NMV of cobosons in the ground state does not exhibit a BEC phase transition, it is still interesting to compare its thermal behaviour with respect to a two-level system occupied by N cobosons.

The thermal state of this system reads

$$
\begin{aligned}
\rho \;=\;& \frac{1}{Z} \sum_{n=0}^{N} e^{-\beta n E_0} e^{-\beta(N-n)E_1} \\
& |n, N-n\rangle\langle n, N-n|,
\end{aligned}
\tag{5.10}
$$

where the total number of cobosons is N and

$$
|n, N-n\rangle = \frac{(\hat{c}_0^\dagger)^n}{\sqrt{\chi_n n!}} \frac{(\hat{c}_1^\dagger)^{N-n}}{\sqrt{\chi_{N-n}(N-n)!}} |0, 0\rangle,
$$

$$
Z = \sum_{n=0}^{N} e^{-\beta n E_0} e^{-\beta(N-n)E_1},
$$

where $\beta = 1/(k_B T)$ and χ_n (χ_{N-n}) is a normalization constant [105]. E_0 and E_1 denote

the energy levels. We derive the NMV of cobosons in the ground state as

$$\langle \hat{n}_0 \rangle = Tr[\hat{c}_0^\dagger \hat{c}_0 \rho] \tag{5.11}$$

$$= \frac{1}{Z} \sum_{n=0}^{N} e^{-\beta n E_0} e^{-\beta (N-n) E_1} [1 + (n-1) \frac{\chi_{n+1}}{\chi_n}].$$

Putting $E_0 = 0$ and $E_1 = 1$, the Eq. (11) becomes

$$\langle \hat{n}_0 \rangle = \frac{1}{Z} \sum_{n=0}^{N} e^{-\beta (N-n)} [1 + (n-1) \frac{\chi_{n+1}}{\chi_n}], \tag{5.12}$$

where the partition function Z is given by $\frac{1-e^{-\beta(N+1)}}{1-e^{-\beta}}$. For a Gaussian state, the normalization ratio is given by Eq. (6). When a pair of fermions is not entangled ($x = 0$), the NMV of cobosons in the ground state becomes equal to one, regardless of temperature. Note that the phenomenon is not possible in the two-level system because every pair of fermions occupies different energy levels. In the two-level system, thus, it is hard to consider pairs of fermions experiencing Pauli exclusion principle. When a pair of fermions is maximally entangled ($x = 1$), the NMV of cobosons in the ground state is given by

$$\langle \hat{n}_0 \rangle_{x=1} = \frac{1}{1 - e^{-\beta(N+1)}} [N - \frac{e^{-\beta}(1 - e^{-\beta N})}{1 - e^{-\beta}}] \tag{5.13}$$

$$\xrightarrow{\beta \to \infty} N.$$

Hence for maximally entangled fermions the $\langle \hat{n}_0 \rangle$ converges to N as temperature tends to zero. In this case the cobosons behave like elementary bosons. The NMV of cobosons is equal to the total mean occupation number of cobosons (N) so that all the cobosons occupy the ground state.

For near maximal entanglement ($K \gg N$) between a pair of fermions, we can derive the analytical result by taking the normalization ratio $\chi_{n+1}/\chi_n \approx 1 - n/K$ [105]. As $T \to 0$ ($\beta \to \infty$), the $\langle \hat{n}_0 \rangle$ is given by

$$\langle \hat{n}_0 \rangle = \langle \hat{n}_0 \rangle_{x=1} - \frac{N}{K(1 - e^{-\beta(1+N)})} [N - 1 - \frac{2e^{-\beta}}{1 - e^{-\beta}} + \frac{2e^{-\beta}(1 - e^{-\beta N})}{N(1 - e^{-\beta})^2}]$$

$$\xrightarrow{T \to 0} N - \frac{N(N-1)}{K} \geq 0$$
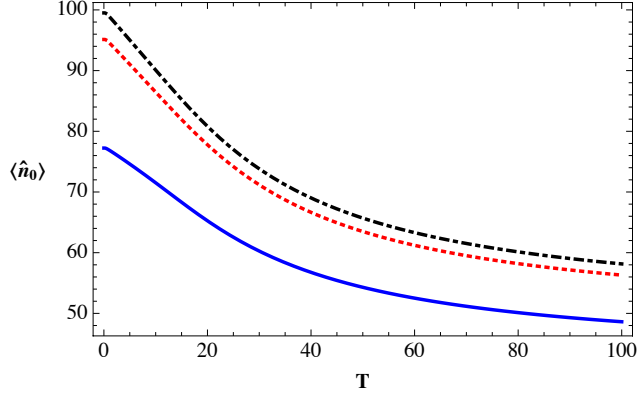
Figure 5.2: NMV of $N = 100$ cobosons in a two-level system as a function of T: from the bottom to the top ($x = 0.995,\ 0.999,\ 0.9999$).

where the Schmidt number K is represented by the parameter x in Eq. (8). From Eq. (8) and the condition $K \gg N$, the parameter x has the following range $1 - x \ll \frac{N-1}{N+1}$. For $N = 100$ we have $1 - x \ll 0.98$. When the Schmidt number K goes to infinity, then the $\langle \hat{n}_0 \rangle$ goes to one. All the cobosons occupy the ground state energy level E_0.

In Fig. 2 we plot the $\langle \hat{n}_0 \rangle$ as a function of T against the range of $1 - x \ll 0.98$. The $\langle \hat{n}_0 \rangle$ increases with the degree of entanglement as well as with decreasing temperature. This coincides with the behaviour of an ideal bosonic gas. As $T \to \infty$, the $\langle \hat{n}_0 \rangle$ of cobosons being perfect bosons is saturated with $N/2$. When x is slightly less than 1, the saturation value of cobosons for $T \to \infty$ can be less than $N/2$. Note that $\langle \hat{n}_0 \rangle < N/2$ is not available in the two-level system because there is no way for the number of particles inverted in equilibrium. Due to the reason, it makes sense to consider BEC in a multi-level system.

5.3.2   Multi-level system: Realistic model

Let us now consider a more realistic physical system consisting of cobosons distributed over the infinitely many energy levels of a 3D isotropic harmonic trap, see Fig. 1 (b). We fix the average number of cobosons to be $\langle \hat{N} \rangle = N$ and describe the system via a grand canonical ensemble with a chemical potential μ. In this paper we do not take the proper thermodynamical limit (such a limit cannot be attained in real experiments) and thus we cannot observe a genuine BEC phase transition. Instead, we follow Mullin [124] and investigate the "pseudo-critical" temperature T_0 below which the increase in the chemical

54
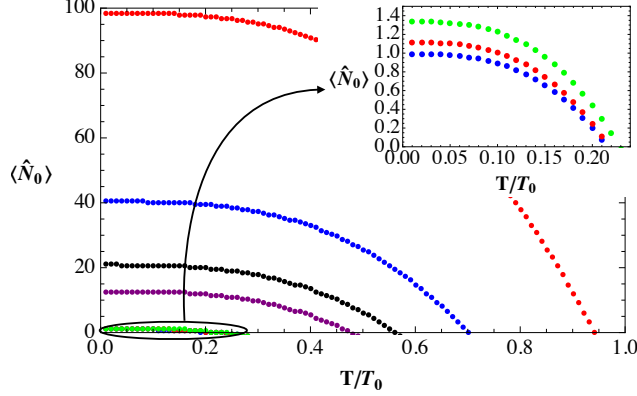
Figure 5.3: NMV of an average number of $N = 100$ cobosons in a multi-level system as a function of T/T_0: from the top to the bottom ($x = 0.9999, 0.99, 0.98, 0.97, 0.8, 0.7, 0.001$). The small box on the right-side corner represents the $\langle \hat{N}_0 \rangle$ for $x = 0.8, 0.7, 0.001$.

potential slows and the number of particles in the ground state begins increasing rapidly (this is also known as the *accumulation point*).

In the grand canonical ensemble, the number-operator mean value (NMV) of the m-th energy level E_m and the total NMV are given by

$$
\langle \hat{N}_m \rangle = \frac{1}{Z_m} \sum_{n=0}^{\infty} e^{-\beta(E_m - \mu)n} [1 + (n-1)\frac{\chi_{n+1}}{\chi_n}],
$$
$$
N = \sum_{m=0}^{\infty} \langle \hat{N}_m \rangle, \tag{5.14}
$$

where $\hat{N}_m = \hat{c}_m^\dagger \hat{c}_m$ and $Z_m = (1 - e^{-\beta(E_m - \mu)})^{-1}$. The energy levels in the 3D isotropic harmonic potential are given by $E_m = \hbar\omega(m_x + m_y + m_z + 3/2)$, where $m_x, m_y, m_z = 0, 1, 2...$ The normalization ratio is given by Eq. (6). When a pair of fermions is not entangled ($x = 0$), the NMV in the ground state is given by

$$
\langle \hat{N}_0 \rangle = \frac{1}{e^{-\beta\mu} - 1} - (1 - e^{\beta\mu}) \sum_{n=0}^{\infty} e^{\beta\mu n}(n-1) = 1, \tag{5.15}
$$

where the energy E_0 has been taken to be zero. It exhibits that only one pair of fermions stay on the ground state energy level E_0, irrespective of T. Note that we cannot find

any temperature dependance of $\langle \hat{N}_0 \rangle$ for $x = 0$. When a pair of fermions is maximally entangled ($x = 1$), the NMV of the ground state energy level becomes the same as the Bose-Einstein distribution. In this scenario we perfectly recover the conventional Bose-Einstein condensation results.

For all regime of x ($0 < x < 1$), the NMV of cobosons in the ground state can be numerically estimated using the approximations,

$$\langle \hat{N}_0 \rangle \approx \langle \hat{N}_0 \rangle_{\alpha \sim 1/N} - N (\frac{T}{T_0})^3 S, \tag{5.16}$$

$$\langle \hat{N}_0 \rangle_{\alpha \sim \frac{1}{N}} = (1 - e^{-1/N}) \sum_{n=1}^{\infty} e^{-n/N} [1 + (n-1) \frac{\chi_{n+1}}{\chi_n}],$$

$$S = \sum_{n=1}^{\infty} (\frac{1}{n^3} - \frac{e^{-1/N}}{(1+n)^3}) e^{-n/N} [1 + (n-1) \frac{\chi_{n+1}}{\chi_n}],$$

where S approaches $\zeta(3) = \sum_{p=1}^{\infty} \frac{1}{p^3} \approx 1.202$ as $N \to \infty$ and $x \to 1$, i.e., for an infinite number of maximally entangled cobosons. The mean value $\langle \hat{N}_0 \rangle_{\alpha \sim 1/N}$ satisfies the boundary conditions, $\langle \hat{N}_0 \rangle_{\alpha \sim 1/N} \approx 1$ at $x \sim 0$ (almost no entanglement) and $\langle \hat{N}_0 \rangle_{\alpha \sim 1/N} \approx N$ at $x = 1$ (maximal entanglement). For near maximal entanglement between the two constituent fermions, the detailed calculations are given in the Appendix.

We plot the NMV of cobosons in the ground state $\langle \hat{N}_0 \rangle$ as a function of T/T_0 for different x in Fig. 3. The $\langle \hat{N}_0 \rangle$ increases with decreasing temperature as well as with the degree of entanglement between the two constituent fermions. At $T/T_0 \sim 0$, we find that as the entanglement approaches 0, the $\langle \hat{N}_0 \rangle$ converges to 1. It is possible that only one pair of fermions occupy the ground state whereas the rest of pairs of fermions occupy all the different energy levels. Thus, different from the two-level system, we can observe the $\langle \hat{N}_0 \rangle$ in all regime of x. In Fig. 3, we can also see that the transition temperature is an increasing function of entanglement, where we have defined the transition temperature as the point at which there are no cobosons in the ground state. This reflects the fact that the $\langle \hat{N}_0 \rangle$ increases with the degree of entanglement.

We can find that our model has some similarities with the references [146, 6]. In the reference [146], for a Gaussian state, the maximum occupation number is approximated as $2(W/v)^3$, where W is the width of the one-boson state and v is the width of the fermion distribution inside one boson. So the maximum occupation number increases with the width of the one-boson state. In our model, the number-operator mean value (NMV) of bifermions in the ground state increases with the entanglement between the two constituent fermions. The entanglement corresponds to the width of the one-boson state, such that the

56

NMV of bi-fermions in the ground state corresponds to the maximum occupation number at $T \to 0$. In the reference [6], which is about N quons that interpolate between bosonic and fermionic statistics, the condensate depletion is represented by $(N - N_0)/N_0$. N_0 is given by $1 - q^N/(1 - q)$, in which $q = 1(-1)$ for boson (fermion). For $q = 1$ (boson), the condensate depletion is equal to 0 which corresponds to our result that all the cobosons are in the ground state at $T \to 0$. For $q = -1$ (fermion), the condensate depletion for odd N is equal to $N - 1$ which also corresponds to our result that only one pair of fermions stay on the ground state at $T \to 0$.

As an example, we consider how T_0 (pseudo-critical temperature) and T_c (critical temperature) are different in a BEC comprised of atomic hydrogen gas for which T_c^e (experimental critical temperature) was observed at $50\mu K$ [61]. Given the density of the hydrogen BEC ($n = 1.8 \times 10^{20} m^{-3}$), the corresponding theoretical critical temperature in the thermodynamic limit is obtained as $T_c^t = \frac{h^2}{2\pi m k_B}(\frac{n}{\zeta(3/2)})^{2/3} \approx 51\mu K$. Since the theoretical critical temperature is derived for ideal BEC, the corresponding pseudo-critical temperature is obtained as $T_0^t = T_c^t[\zeta(3)]^{1/3} \approx 54.06\mu K$. For the experimental critical temperature, the pseudo-critical temperature is derived as a function of the degree of entanglement between the proton and electron. Using the purity of the proton $P = \frac{33}{4\sqrt{2\pi}}(\frac{a_0}{b})^3$ [32] with the experimental trapping size ($b \approx 9.6 \times 10^{-8} m$), we find that the proton and the electron are highly entangled with the purity $P \sim 10^{-10}$ while the maximum entanglement is obtained at $P = 0$. Thus, using the relation $(T/T_0)^3\zeta(3) \approx (T/T_c)^3$, the corresponding pseudo-critical temperature is derived as $T_0^e = T_c^e[\zeta(3)]^{1/3} \approx 53.16\mu K$. Therefore, we see that our pseudo-critical temperature is a good approximation for the critical temperature.

5.4   Bi-boson: a pair of bosons

We consider cobosons comprised of two bosons (bi-boson). For a Gaussian state, the normalization ratio is represented by Eq. (7). Here x parametrizes the degree of entanglement between a pair of bosons. An example of a coboson is a bi-photon generated by spontaneous parametric down conversion, which exhibits composite behavior even if the two photons are spatially separated [105]. To keep bi-photons together, we can consider a dye solution which repeatedly absorbs and re-emits photons [93]. Previously bi-bosons were considered for super-bunching effect [102, 173].

5.4.1 Two-level system: Simplified model

We consider a two-level system with a fixed number of N cobosons. All the formulas used in the previous section are applied here as well - the only difference is the normalization ratio χ_{n+1}/χ_n. As we mentioned in Sec. II, due to the bunching effect between the two constituent bosons, the number-operator mean value (NMV) of cobosons can be larger than the total mean occupation number of cobosons (N) when the degree of entanglement between the two constituent bosons is quantified by a value of $x < 1$.

When a pair of bosons is not entangled ($x = 0$), from Eq. (12) the NMV of cobosons in the ground state is given by

$$\langle \hat{n}_0 \rangle_{x=0} = \frac{N}{1 - e^{-\beta(1+N)}}[N - \frac{2e^{-\beta}}{1 - e^{-\beta}} + \frac{e^{-\beta}(1 + e^{-\beta})(1 - e^{-\beta N})}{N(1 - e^{-\beta})^2}] \xrightarrow{T \to 0} N^2, \quad (5.17)$$

where $\beta = 1/(k_B T)$. Hence for separable bosons the $\langle \hat{n}_0 \rangle_{x=0}$ converges to N^2 as temperature tends to zero. Although the cobosons are no longer behaving like ideal bosons, the dissociated components of each bi-boson pair will both independently exhibit bosonic behavior. This causes the $\langle \hat{n}_0 \rangle$ to increase as the entanglement between the two constituent bosons decreases. We can see this directly from the formula for $\hat{c}^\dagger$ in Eq. (5). At $x = 0$ (no entanglement), the coboson operator is represented by $\hat{c}^\dagger = \hat{a}^\dagger \hat{b}^\dagger$. As $T \to 0$, from Eq. (12), the state of cobosons in the ground state can be described by the coboson number state $|N\rangle$. So the NMV of the cobosons in the ground state is given by

$$\langle N | \hat{c}^\dagger \hat{c} | N \rangle = \langle N_a, N_b | \hat{a}^\dagger \hat{a} \hat{b}^\dagger \hat{b} | N_a, N_b \rangle = N^2, \quad (5.18)$$

where a and b represent different modes. Note that the NMV of bi-bosons is not same as the mean occupation number of the dissociated components of bi-bosons ($2N$) at $x = 0$. It can be explained that the enormous value N^2 comes out of the sum of the correlation functions in Eq. (9), where the correlations functions can exhibit super-bunching effects by wave nature. When a pair of bosons is maximally entangled ($x = 1$), the $\langle \hat{n}_0 \rangle$ converges to N as temperature goes to zero.

For near maximal entanglement ($K \gg N$) between a pair of bosons, we can make the approximation, $\chi_{n+1}/\chi_n \approx 1 + n/K$ [105]. As $T \to 0$, the $\langle \hat{n}_0 \rangle$ approaches

$$\langle \hat{n}_0 \rangle = \langle \hat{n}_0 \rangle_{x=1} + \frac{N}{K(1 - e^{-\beta(1+N)})}[N + 1 - \frac{2e^{-\beta}}{1 - e^{-\beta}} + \frac{2e^{-2\beta}(1 - e^{-\beta N})}{N(1 - e^{-\beta})^2}]$$

$$\xrightarrow{T \to 0} N + \frac{N(N+1)}{K} \geq N,$$

Figure 5.4: NMV of $N = 100$ cobosons in a two-level system as a function of T/T_0: from the bottom to the top ($x = 0.9999$, 0.99, 0.8, 0.7, 0.5, 0.2, 0.001). The small box on the right-side corner represents the condensate fraction for $x = 0.9999$, 0.99. Here x represents the degree of entanglement for a pair of bosons.

where $\langle \hat{n}_0 \rangle_{x=1}$ is given by Eq. (13). If the Schmidt number K goes to infinity, then the $\langle \hat{n}_0 \rangle$ goes to N. For all regimes of x ($0 < x < 1$), we plot the $\langle \hat{n}_0 \rangle$ as a function T in Fig. 4. The $\langle \hat{n}_0 \rangle$ decreases with increasing temperature as well as with the degree of entanglement between the two constituent bosons. At $T \sim 0$, the $\langle \hat{n}_0 \rangle$ is maximized as a decreasing function of entanglement which ranges from N^2 to N. In contrast to cobosons comprised of fermions, therefore, the $\langle \hat{n}_0 \rangle$ decreases with entanglement between the two constituent bosons, due to the super-bunching effects between the two constituent bosons.

5.4.2 Multi-level system: Realistic model

We consider a 3D isotropic harmonic trap which contains an average of N cobosons. When a pair of bosons is not entangled ($x = 0$), the NMV of the ground state in Eq. (15) is given by

$$\langle \hat{N}_0 \rangle = \frac{1}{Z_0} \sum_{n=0}^{\infty} e^{-\beta(E_0 - \mu)n} n^2 = \frac{z(1+z)}{(1-z)^2}, \tag{5.19}$$

where $z = \exp(\beta\mu)$ is the fugacity and E_0 has been taken to be zero. Compared with the Bose-Einstein (BE) distribution where $N_0 = z/(1-z)$, the $\langle \hat{N}_0 \rangle$ is always greater than the BE distribution one. When a pair of bosons is maximally entangled ($x = 1$), the $\langle \hat{N}_0 \rangle$ is the same as for BE distribution. This reaffirms the potential for BEC of bi-bosons.
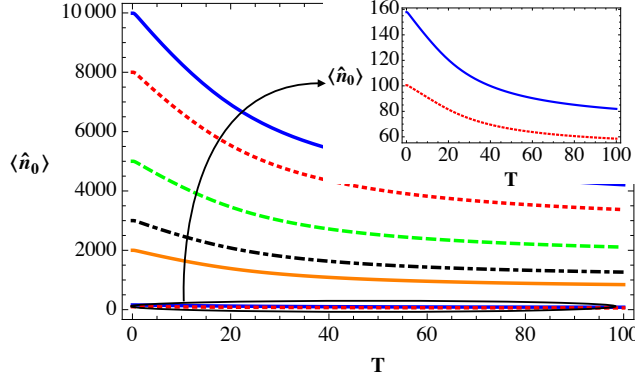
59
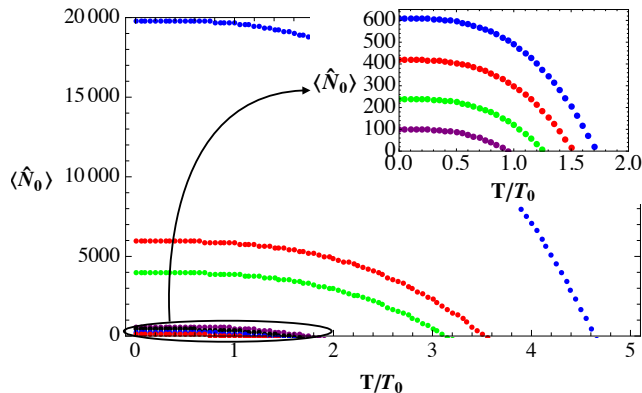
Figure 5.5: NMV of an average number of $N = 100$ cobosons in a multi-level system as a function of T/T_0: from the bottom to the top ($x = 0.9999$, 0.99, 0.98, 0.97, 0.8, 0.7, 0.001). The small box on the right-side corner represents the condensate fraction for $x = 0.9999$, 0.99, 0.98, 0.97. Here x represents the degree of entanglement for a pair of bosons.

In Fig. 5 we plot the $\langle \hat{N}_0 \rangle$ as a function of T/T_0, for bi-bosons exhibiting a range of entanglement values. The $\langle \hat{N}_0 \rangle$ decreases with the degree of entanglement between the two constituent bosons. As bi-bosons become less entangled they behave more like a system of two independent bosons. Hence at $T/T_0 \sim 0$, the $\langle \hat{N}_0 \rangle$ is maximized as a decreasing function of entanglement. Using Eq. (20), we derive the maximum condensate fraction at $x \sim 0$ as

$$\langle \hat{N}_0 \rangle_{x=0} = (1 - e^{-1/N}) \sum_{n=1}^{\infty} e^{-n/N} n^2 \approx 2N^2, \tag{5.20}$$

where N is sufficiently large. In Fig. 5, we can also see that the transition temperature decreases with increasing entanglement. This reflects the fact that the $\langle \hat{N}_0 \rangle$ decreases with the degree of entanglement. Therefore, similarly to the two-level system, we observe that the $\langle \hat{N}_0 \rangle$ decreases as a function of entanglement between the two constituent bosons.

We have never experimentally observed the phenomenon of bi-boson BEC, but a BEC experiment has been conducted using photons in an optical micro-cavity [93]. Based on the techniques used to create a BEC from photons, we look forward to observing future bi-photon condensates in optical cavities.

60

5.5   Conclusion

We studied how the deviation from ideal bosonic behavior exhibited by cobosons affects BEC. We specifically consider bi-fermions trapped in a two-level system or a 3D isotropic harmonic system. By the Pauli exclusion principle between bi-fermions, we figured out that the number-operator mean value (NMV) of bi-fermions is the same as the mean occupation number (MON) of bi-fermions in the 3D isotropic harmonic system. We demonstrated that the (NMV) of bi-fermions in the ground state is an increasing function of entanglement between a pair of fermions, where the whole regime of the entanglement parameter ($0 < x < 1$) could be investigated only in the 3D isotropic harmonic system due to the Pauli exclusion principle. Heuristically the higher the level of entanglement between a pair of fermions the more bosonic the bi-fermions behave. Correspondingly, we found that the transition temperature for the 3D isotropic harmonic system, i.e., the temperature at which all the bi-fermions moved to the excited states, is an increasing function of entanglement.

Furthermore, we discussed coboson BEC, where each coboson is a bi-boson. Due to the bunching effect between a pair bosons, we figured out that the NVM of bi-bosons can be larger than the total MON of bi-bosons, regardless of system. Surprisingly it was shown that the NMV of bi-bosons in the ground state decreases with the degree of entanglement between a pair of bosons, due to the bunching effect between a pair of bosons. As the entanglement parameter (x) increased from 0 to 1, the NMV of bi-bosons in the ground state decreased for $T < T_0$ in the 3D isotropic harmonic system. The higher the entanglement the more closely the bi-bosons imitated indivisible bosons. When the entanglement between a pair of bosons became sufficiently small, the bi-boson pairs dissociated, increasing the bunching effect in the NMV of bi-bosons. Correspondingly, the transition temperature for the 3D isotropic harmonic system decreased with increasing entanglement.

This may open a new avenue for detecting entanglement at the microscopic level using a macroscopic measurement. In other words, the condensation rate could be used as a witness for entanglement.

Another direction to explore is to study composite particles that involve more than two entities. Clearly, it is more complicated to study these kinds of composite particles due to the lack of Schmidt decomposition. However, it would be interesting to see if some of the tools from quantum information and entanglement theory may be exploited to characterise these kinds of particles.

and IQC.

Chapter 6

Entropic Version of the Greenberger-Horne-Zeilinger Paradox

Most of the content of this chapter was published in [137]. I proposed the main idea of the paper and did some of the calculations, and double checked the rest of them. I also contributed in writing the paper.

6.1 Introduction

It was first observed by Bell [12] that bipartite quantum systems can violate local realism and later this observation was extended to multipartite systems [119, 3, 11]. It was also shown that for more than two particles it is possible to formulate the Greenberger-Horne-Zeilinger (GHZ) paradox [74], that is an all-versus-nothing contradiction of local realism, in a sense that it employs deterministic measurement outcomes. Around the same time it was shown that the local realism of bipartite systems can be studied using the notion of Shannon entropy and the bipartite information-theoretic Bell inequalities were proposed [23]. However, multipartite entropic inequalities have not been constructed up to now. In this work we extend the previous results, provide a tripartite information-theoretic Bell inequality and formulate an entropic version of the GHZ paradox.

6.1.1 GHZ Paradox

The original GHZ paradox [74] occurs in multipartite quantum systems. In a simplest scenario one considers a system of three qubits in the GHZ state

$$|GHZ\rangle = \frac{1}{\sqrt{2}}(|000\rangle + |111\rangle) \tag{6.1}$$

and four observables $A = YYX$, $B = YXY$, $C = XYY$ and $D = XXX$, where X and Y are Pauli operators (whose measurement outcomes are ± 1) and we used the simplified notation $XXX \equiv X \otimes X \otimes X$. Any local realistic theory that assigns measurement outcomes to local observables (deterministic) necessarily predicts that the product $ABCD = 1$, since in this product each ± 1 observable X and Y occurs twice. However, for the GHZ state all four observables are determined and are $A = -1$, $B = -1$, $C = -1$ and $D = 1$ which contradicts local realistic predictions.

Here, we show that similar all-versus-nothing contradiction can be formulated in terms of information. In particular, we define four observables A, B, C and D for which classical reasoning predicts that if we have full knowledge of A, B and C, then we automatically have full knowledge of D. However, for the GHZ state one has full knowledge of A, B, C and at the same time no knowledge of D at all.

6.1.2 Triangle Principle

We use the previously developed information-theoretic distance approach to nonclassical correlations [100, 156] and propose a new distance-like property that can be applied to binary ± 1 measurements. This property quantifies multipartite correlations in terms of Shannon entropy and can be applied to derive a tripartite inequality whose structure resembles the tripartite Mermin inequality [119]. However, in our case we relate entropies of multipartite measurement outcomes, not multipartite correlation functions like in Ref. [119]. The inequality is satisfied whenever the information-theoretic distance-like property applies to the system (which is true for example in case of classical local realistic systems), but is violated by measurements on quantum systems. Interestingly, our tripartite inequality can be maximally violated within quantum theory, which does not happen in the bipartite case [23]. Due to this fact, our inequality can be interpreted as an entropic version of the GHZ paradox.

The information-theoretic distance was originally proposed by Zurek [190]. Initially, it was defined using the notion of Kolmogorov entropy, but it can be also defined via Shannon

entropy [100, 156] as

$$d(A, B) = H(A|B) + H(B|A), \tag{6.2}$$

where A and B are random variables, $H(A|B) = H(AB) - H(B)$ is the conditional Shannon entropy, $H(B)$ is the entropy of the variable B and $H(AB)$ is the joint entropy of A and B. It can be shown that $H(A|B) + H(B|A)$ satisfies all of the requirements of a distance [100].

The information-theoretic Bell inequalities can be constructed via multiple application of the triangle inequality [100], e.g., $d(A, B) \leq d(A, B') + d(B, B')$ and $d(B, B') \leq d(A', B') + d(A', B)$ give

$$d(A, B) \leq d(A, B') + d(A', B') + d(A', B). \tag{6.3}$$

Here, $\{A, A'\}$ and $\{B, B'\}$ label different measurable properties of Alice's and Bob's systems, respectively, and $d(A, B)$, $d(A, B')$, ... are information-theoretic distances between them. The natural intuition behind this inequality is that the shortest path goes directly from A to B and if one chose to go around through B' and A' one would have to take a longer route. The violation of such inequalities indicates that the system does not obey some properties of a metric and it was shown that this can happen for quantum systems [100, 156].

The notion of a distance is designed as a property between two points. In the information-theoretic framework a distance describes a relation between two random variables – in our case, two jointly measurable observables. It is therefore somehow unnatural to expect that the same framework can be adopted for three or more jointly measurable properties. However, here we show that this can be done.

The rest of the chapter is organised as follows. First, we introduce an information-theoretic distance-like property that applies to more than two measurements. Next, we use this property to derive a tripartite information-theoretic Bell inequality. Then, we show that this inequality can be maximally violated within quantum theory and interpret it as an entropic version of the GHZ paradox. Finally, we discuss our results and suggest further avenues of research on this topic.

Distance-like property. Let us consider the following function defined for binary observables A and B

$$d(A, B) = H(A \cdot B), \tag{6.4}$$

where $H(.)$ is the Shannon entropy, i.e. $-p_{+1} \log(p_{+1}) - p_{-1} \log(p_{-1})$ for outcomes ± 1 with different probabilities $p_{\pm 1}$. Before we proceed, we should emphasis that this function is a distance only if the outcomes of A and B are ± 1. The measurement of $A \cdot B$ is one where

the outcomes are the product of the outcomes of A and B, i.e. if the outcome of A is a and the outcome of B is b , then the outcome of $A \cdot B$ is ab.

The function in Eq.(6.4) satisfies all of the following properties.

1. $d(A, A) = H(A \cdot A) = 0$ because the outcome of this measurement is always one and $d(A, B) \geq 0$ because $H(X) \geq 0, \forall X$.

2. $d(A, B) = d(B, A)$.

3. The triangle inequality: $H(A \cdot B) \leq H(B \cdot C) + H(A \cdot C), \forall A, B, C$.

The triangle inequality is satisfied because

$$H(A \cdot B | A \cdot C, B \cdot C) = 0, \tag{6.5}$$

In other words, if the outcomes of the two measurements $A \cdot C$ and $B \cdot C$ are known, then the outcome of $A \cdot B$ is the product of the two outcomes and is therefore known. More precisely,

$$H(A \cdot B) \leq H(A \cdot B, B \cdot C, A \cdot C) = H(A \cdot B | A \cdot C, B \cdot C) + H(B \cdot C, A \cdot C) \tag{6.6}$$
$$= H(B \cdot C, A \cdot C) \leq H(B \cdot C) + H(A \cdot C). \tag{6.7}$$

In the above we used the facts that $H(AB) = H(A|B) + H(B)$, $H(AB) \leq H(A) + H(B)$ and $H(A) \leq H(AB)$.

The distance in Eq. (6.4) can simply be extended to a distance-like property for the multipartite measurements. Note that for a set of operators $\{A_1, A_2, \ldots, A_n\}$ one can define

$$\delta(A_1, A_2, \ldots, A_n) = H(A_1 \cdot A_2 \cdot \ldots \cdot A_n), \tag{6.8}$$

which is the natural extension of the distance for two operators. We need this later to find the multi-partite Mermin-like inequality.

Tripartite information-theoretic Bell inequality. Let us examine the properties of (6.8) in the context of multipartite measurements. For multipartite measurements, A_i would be the local observable. Within quantum theory this measurement would be represented by the local A_i operator for the specific party conjugated with the identity operators for other parties. For instance, for the measurement of A for Alice and B for Bob and C

for Charlie one would have $A_1 = A \otimes \mathbb{I} \otimes \mathbb{I}$, $A_2 = \mathbb{I} \otimes B \otimes \mathbb{I}$, $A_3 = \mathbb{I} \otimes \mathbb{I} \otimes C$ leading to $\delta(A_1, A_2, A_3) = H(A \otimes B \otimes C)$.

The function δ is obviously symmetric, but it also has a nice associative property which is

$$\delta(A_1, A_2, A_3) = d(A_1, (A_2 \cdot A_3)). \tag{6.9}$$

This comes from the fact that $H(A_1 \cdot A_2 \cdot A_3) = H(A_1 \cdot (A_2 \cdot A_3))$. Note that using to the symmetry property, any two A_i could be associated.

Now we derive the following inequality:

$$\begin{aligned} \delta(A_1, B_1, C_1) &\leq \\ \delta(A_1, B_2, C_2) &+ \delta(A_2, B_2, C_1) + \delta(A_2, B_1, C_2). \end{aligned} \tag{6.10}$$

The derivation is as follows:

$$\begin{aligned} \delta(A_1, B_1, C_1) &\leq d(A_1, (B_2.C_2)) + d((B_2.C_2), (B_1.C_1)) \\ &= d(A_1, B_2.C_2) + \delta(B_2, C_1, B_1, C_2) \\ &\leq \delta(A_1, B_2, C_2) + d(A_2, B_2 \cdot C_1) + d(A_2, B_1 \cdot C_2) \\ &= \delta(A_1, B_2, C_2) + \delta(A_2, B_2, C_1) + \delta(A_2, B_1, C_2). \end{aligned}$$

The first and the last inequalities come from using the triangle inequality with $B_2 \cdot C_2$ and A_2 respectively and equality in the middle comes from the symmetry property.

Note that the derivation holds not only for the function δ, but for any distance with the associativity property in (6.9). For instance, applying the generalisation of the co-variance distance [100, 156], $\delta(A_1, A_2, A_3) = 1 - \langle A_1 \cdot A_2 \cdot A_3 \rangle$ to the inequality (6.10) gives the original tripartite Mermin inequality [119].

The inequality (6.10) was derived using the classical properties of Shannon entropy, therefore it must hold in any theory that obeys them. In particular, in local realistic theories there exists a joint probability distribution for all observables $A_1, \ldots, C_2$ [60] and as a consequence there exists a joint entropy $H(A_1 \ldots C_2)$ which implies the validity of (6.10). However, one may expect the violation of this inequality if a theory does not admit a joint probability distribution.

6.2   Quantum violation and the paradox

Let us consider a three-qubit system in a GHZ state $|GHZ\rangle = \frac{1}{\sqrt{2}}(|000\rangle + |111\rangle)$ shared between Alice, Bob and Charlie. Each of them performs one of the two possible local

measurements on their subsystem: $A_1, A_2, B_1, \dots$ As previously discussed, we can choose $\delta(A_i, B_j, C_k) = H(A_i \otimes B_j \otimes C_k)$ (for $i, j, k = 1, 2$) and plug these measurements to the inequality (6.10) to obtain

$$
\begin{aligned}
H\left(A_1 \otimes B_1 \otimes C_1\right) &\leq H\left(A_1 \otimes B_2 \otimes C_2\right) \\
&+ H\left(A_2 \otimes B_1 \otimes C_2\right) + H\left(A_2 \otimes B_2 \otimes C_1\right).
\end{aligned}
\tag{6.11}
$$

Note that $A_i \otimes B_j \otimes C_k$ are binary ± 1 observables, therefore $H(A_i \otimes B_j \otimes C_k)$ cannot exceed one. If this entropy is equal to one, then we have no knowledge of $A_i \otimes B_j \otimes C_k$ and if it is zero, we are certain about the value of this observable. To simplify the notation we set $A \equiv A_1 \otimes B_2 \otimes C_2$, $B \equiv A_2 \otimes B_1 \otimes C_2$, $C \equiv A_2 \otimes B_2 \otimes C_1$ and $D \equiv A_1 \otimes B_1 \otimes C_1$. The inequality (6.11) takes form

$$
H(D) \leq H(A) + H(B) + H(C).
\tag{6.12}
$$

It bounds the entropy of D via the entropies of A, B and C. In particular, it predicts that if A, B and C are known (their entropy is zero), then D must be known too. An additional argument for that is along the GHZ reasoning — if the outcomes are predetermined, then the values of A, B, C and D (denoted as a, b, c and d) must multiply to one ($abcd = 1$). Therefore, if we know A, B and C, we automatically know D, since $d = abc$.

However, quantum theory allows for a violation of the inequality (6.12). If Alice, Bob and Charlie chose

$$
\begin{aligned}
A_1 = B_1 = C_1 &= \cos\left(\frac{\pi}{6}\right) X + \sin\left(\frac{\pi}{6}\right) Y, \\
A_2 = B_2 = C_2 &= \cos\left(\frac{\pi}{12}\right) X - \sin\left(\frac{\pi}{12}\right) Y,
\end{aligned}
\tag{6.13}
$$

they would observe that $H(A) = H(B) = H(C) = 0$, but at the same time $H(D) = 1$. We achieved maximal algebraic violation and observed that although A, B and C are known, D is completely unknown!

6.3 Test via compression

The plausible feature of the original GHZ paradox is that it does not involve probabilities, despite the fact that quantum theory is fundamentally probabilistic. Here, the entropies $H(A)$, $H(B)$ and $H(C)$ are zero, therefore the corresponding measurement events are fully predetermined. On the other hand, $H(D) = 1$ indicates that D is maximally random. Still

the entropic GHZ paradox can be investigated without invoking quantum probabilities by using the data compression approach proposed in [101].

Imagine that Alice, Bob and Charlie perform n rounds of measurements A_i, B_j and C_k, respectively. They produce bit strings $a^{(i)} = a_1^{(i)} a_2^{(i)} \ldots a_n^{(i)}$, $b^{(j)} = b_1^{(j)} b_2^{(j)} \ldots b_n^{(j)}$, and $c^{(k)} = c_1^{(k)} c_2^{(k)} \ldots c_n^{(k)}$. Due to the fact that each measurement round is performed on a different independent triple of qubits prepared in the GHZ state, the subsequent bits in each string are independent and identically distributed (i.i.d.). In this case, the expression $nH(A_i \otimes B_j \otimes C_k)$ is the Shannon entropy of a bit string that is a concatenation (XOR) of bit strings $a^{(i)}$, $b^{(j)}$ and $c^{(k)}$, i.e. $H(a^{(i)} \oplus b^{(j)} \oplus c^{(k)})$.

For i.i.d. bit strings Shannon entropy gives the best possible compression rate [42]. In case of real life compressors, like gzip or Huffman code, the compression rate is worse than the Shannon entropy. Still, for uniform (deterministic) bit strings $a^{(i)} \oplus b^{(j)} \oplus c^{(k)}$ the compression rate $C(a^{(i)} \oplus b^{(j)} \oplus c^{(k)})$ obtained by a real life compressor C is of the order $O(\log n)$ [14, 33]. It is therefore justified to use a modified version of the inequality (6.11)

$$
\begin{aligned}
C(a^{(1)} \oplus b^{(1)} \oplus c^{(1)}) &\leq C(a^{(1)} \oplus b^{(2)} \oplus c^{(2)}) \\
+ \quad C(a^{(2)} \oplus b^{(1)} \oplus c^{(2)}) &+ C(a^{(2)} \oplus b^{(2)} \oplus c^{(1)})
\end{aligned}
\tag{6.14}
$$

as a valid bound on classical theories, if the compression rates on the right hand side are $O(\log n)$. The above inequality will be violated by the quantum measurements discussed in the previous section, because the bit strings on the right hand side are predicted to be uniform, whereas the bit string on the left hand side is predicted to be maximally random, therefore $C(a^{(1)} \oplus b^{(1)} \oplus c^{(1)}) = O(n)$. Although we do not provide the proof, we speculate that the above inequality will be also valid (as a classical bound) in case of experimental noise and for an arbitrary measurement scenario.

Interestingly, the tripartite inequality (6.11) is more robust to noise than the bipartite information-theoretic inequality studied in [23]. In case of the white noise admixture $\mathbb{I}/8$ to the pure GHZ state $\rho(p) = (1-p)|GHZ\rangle\langle GHZ| + p\mathbb{I}/8$, the value of p for which the violation vanishes is $p \approx 0.123$. The corresponding threshold value for the bipartite inequality [23] is $p \approx 0.04$. Of course, this comparison can be only used as a reference, since in reality it is much harder to engineer the tripartite GHZ state than the bipartite singlet state.

6.4   Conclusions

We proposed a tripartite information-theoretic Bell inequality based on a distance-like property. The inequality is maximally violated by measurements on three qubits in the GHZ state and we used this fact to formulate the entropic version of the GHZ paradox. Finally, we discussed the test of this paradox in terms of compressibility of bit strings generated from the measurement data obtained by parties sharing the three qubits and showed that our multipartite scenario is more robust to noise than the corresponding bipartite scenario.

Arguably the entropic inequality may be interpreted to be more fundamental than correlation inequalities because arguably information may be seen as being more fundamental than probabilities [50]. There are even proposals for defining and calculating entropy without probabilities. For instance in thermodynamics one can calculate the entropy using the free energy without knowing the probabilities directly.

Another significance of the entropic inequalities is that they may be easier to be extended to the macroscopic regime. We know from thermodynamics that the microscopic entropy could simply extend to the macroscopic one. Similarly, one may expect that a characterization of quantum mechanics in terms of information may have a smooth transition from the microscopic scale to the macroscopic one.

There are several open problems that require further investigation. First of all, it is natural to look for an extension of our result to more than three parties and to higher-level systems. Moreover, bipartite information-theoretic Bell inequalities are less efficient in detection of the lack of local realism than the correlation based inequalities. It is therefore important to investigate the class of states violating our inequality and to compare this class with the class of states violating the Mermin inequality. It is also interesting to explore this kind of inequalities for more practical informations like Renyi entropies that can be measured experimentally. more Finally, it would be important to prove (or disprove) our conjecture that the inequality (6.14) is always valid.

Chapter 7

Conclusion

I probed the transition between microscopic and macroscopic quantum effects at different levels. As I mentioned in the introduction chapter, quantum systems could have two different kind of macroscopicity: the state could be macroscopic and the measurements could be macroscopic. In this thesis, we gave example of the all four possible situations (See figure 1.1).

We mentioned some of the proposals and experiments for macroscopic measurements on macroscopic quantum states and and pointed out the in most cases, the measurements are highly sensitive to the precision of measurements and coarse-graining. We studied a proposal that was known to be a counter-example to this trend and showed that this proposal also suffer from the high precision requirement, it only requires a different kind of precision, namely, control precision. We also conjectured that this is a general property of all of the macroscopic quantum states. Specifically the conjecture is that a macroscopic measurement of macroscopic states would require a precision that increases with the size of the system, this precision may be in the outcome or control of the measurement, but either ways, it makes the measurement challenging.

We also proposed a solution to go around this problem. We proposed to use a microscopic measurement on a macroscopic measurement and showed that this can be used to demonstrate entanglement between a single photon and a macroscopic state. We also mentioned that idea was exploited experimentally.

We also looked at the Bose-Einstein condensation properties of composite bosons and showed that the condensation rate depends on the entanglement between the entities of the composite particle. This suggests that condensation rate, although a macroscopic

(thermodynamic) behaviour of these systems, can be used to witness entanglement at a microscopic level, between the entities of the composite particle.

At a more abstract level, we also found an entropic Mermin-like inequality which has the potential to be extended for macroscopic systems, although at this point, it only applies to microscopic measurements of microscopic states.

We also solved a ten year old problem related to HBAC, namely the limit of cooling in these methods. We proved the asymptotic state and the cooling limit of the optimal technique of cooling which therefore applies to all the HBAC techniques as well.

References

[1] Armen E. Allahverdyan, Karen V. Hovhannisyan, Dominik Janzing, and Guenter Mahler. Thermodynamic limits of dynamic cooling. *Phys. Rev. E*, 84:041109, Oct 2011.

[2] Mike H. Anderson, Jason R Ensher, Michael R Matthews, Carl E Wieman, and Eric A Cornell. Observation of Bose-Einstein condensation in a dilute atomic vapor. *Science*, 269(5221):198–201, 1995.

[3] M Ardehali. Bell inequalities with a magnitude of violation that grows exponentially with the number of particles. *Physical Review A*, 46(9):5375, 1992.

[4] Jan H. Ardenkjær-Larsen, Björn Fridlund, Andreas Gram, Georg Hansson, Lennart Hansson, Mathilde H. Lerche, Rolf Servin, Mikkel Thaning, and Klaes Golman. Increase in signal-to-noise ratio of $> 10,000$ times in liquid-state NMR. *Proceedings of the National Academy of Sciences*, 100(18):10158–10163, September 2003.

[5] A. Auffeves, P. Maioli, T. Meunier, S. Gleyzes, G. Nogues, M. Brune, J. M. Raimond, and S. Haroche. Entanglement of a mesoscopic field with an atom induced by photon graininess in a cavity. *Phys. Rev. Lett.*, 91:230405, Dec 2003.

[6] S. S. Avancini, J. R. Marinelli, and G Krein. Compositeness effects in the bose–einstein condensation. *Journal of Physics A: Mathematical and General*, 36(34):9045, 2003.

[7] M. D. Barrett, B. DeMarco, T. Schaetz, V. Meyer, D. Leibfried, J. Britton, J. Chiaverini, W. M. Itano, B. Jelenković, J. D. Jost, C. Langer, T. Rosenband, and D. J. Wineland. Sympathetic cooling of 9be+ and 24mg+ for quantum logic. *Phys. Rev. A*, 68:042302, Oct 2003.

[8] Angelo Bassi, Kinjalk Lochan, Seema Satin, Tejinder P Singh, and Hendrik Ulbricht. Models of wave-function collapse, underlying theories, and experimental tests. *Reviews of Modern Physics*, 85(2):471, 2013.

[9] Jonathan Baugh, Osama Moussa, Colm A Ryan, Ashwin Nayak, and Raymond Laflamme. Experimental implementation of heat-bath algorithmic cooling using solid-state nuclear magnetic resonance. *Nature*, 438(7067):470–473, 2005.

[10] N. Behbood, F. Martin Ciurana, G. Colangelo, M. Napolitano, Géza Tóth, R. J. Sewell, and M. W. Mitchell. Generation of macroscopic singlet states in a cold atomic ensemble. *Phys. Rev. Lett.*, 113:093601, Aug 2014.

[11] AV Belinskiĭ and DN Klyshko. Interference of light and bell's theorem. *Physics-Uspekhi*, 36(8):653, 1993.

[12] John S Bell. On the einstein-podolsky-rosen paradox. *Physics*, 1(3):195–200, 1964.

[13] Michael Ben-Or, Daniel Gottesman, and Avinatan Hassidim. Quantum refrigerator. *arXiv preprint arXiv:1301.1995*, 2013.

[14] Charles H Bennett, Péter Gács, Ming Li, Paul MB Vitányi, and Wojciech H Zurek. Information distance. *Information Theory, IEEE Transactions on*, 44(4):1407–1423, 1998.

[15] Gunnar Björk and Piero G. Luca Mana. A size criterion for macroscopic superposition states. *Journal of Optics B: Quantum and Semiclassical Optics*, 6(11):429, 2004.

[16] John M Blatt, KW Böer, and Werner Brandt. Bose-Einstein condensation of excitons. *Physical Review*, 126(5):1691, 1962.

[17] P. Oscar Boykin, Tal Mor, Vwani Roychowdhury, Farrokh Vatan, and Rutger Vrijen. Algorithmic cooling and scalable NMR quantum computers. *Proceedings of the National Academy of Sciences*, 99(6):3388–3393, March 2002. PMID: 11904402.

[18] C. C. Bradley, C. A. Sackett, J. J. Tollett, and R. G. Hulet. Evidence of Bose-Einstein condensation in an atomic gas with attractive interactions. *Physical Review Letters*, 75(9):1687, 1995.

[19] Fernando G. S. L. Brandão, Michał Horodecki, Jonathan Oppenheim, Joseph M. Renes, and Robert W. Spekkens. Resource theory of quantum states out of thermal equilibrium. *Phys. Rev. Lett.*, 111:250404, Dec 2013.

[20] Gilles Brassard. Is information the key? *Nature Physics*, 1(1):2–4, 2005.

[21] Gilles Brassard, Yuval Elias, José M Fernandez, Haggai Gilboa, Jonathan A. Jones, Tal Mor, Yossi Weinstein, and Li Xiao. Experimental heat-bath cooling of spins. *arXiv:1404.6885 [quant-ph]*, April 2014. arXiv: 1404.6885.

[22] Gilles Brassard, Yuval Elias, Tal Mor, and Yossi Weinstein. Prospects and limitations of algorithmic cooling. *arXiv:1404.6824 [quant-ph]*, April 2014. arXiv: 1404.6824.

[23] Samuel L. Braunstein and Carlton M. Caves. Information-theoretic bell inequalities. *Physical review letters*, 61(6):662, 1988.

[24] M. Brune, E. Hagley, J. Dreyer, X. Maî tre, A. Maali, C. Wunderlich, J. M. Raimond, and S. Haroche. Observing the progressive decoherence of the "meter" in a quantum measurement. *Phys. Rev. Lett.*, 77:4887–4890, Dec 1996.

[25] Natalia Bruno, Anthony Martin, Pavel Sekatski, Nicolas Sangouard, Robert Thomas Thew, and Nicolas Gisin. Displacement of entanglement back and forth between the micro and macro domains. *Nature Physics*, 9(9):545–548, 2013.

[26] Dagmar Bruß, Mirko Cinchetti, G Mauro D'Ariano, and Chiara Macchiavello. Phase-covariant quantum cloning. *Physical Review A*, 62(1):012302, 2000.

[27] Dagmar Bruss, Artur Ekert, and Chiara Macchiavello. Optimal universal quantum cloning and state estimation. *Physical review letters*, 81(12):2598, 1998.

[28] Vladimir Bužek and Mark Hillery. Quantum copying: Beyond the no-cloning theorem. *Physical Review A*, 54(3):1844, 1996.

[29] Eric Gama Cavalcanti and M. D. Reid. Criteria for generalized macroscopic and mesoscopic quantum coherence. *Physical Review A*, 77(6):062108, 2008.

[30] J Černỳ and P Brunovskỳ. A note on information without probability. *Information and Control*, 25(2):134–144, 1974.

[31] TK Chuan and Dagomir Kaszlikowski. Composite particles and the szilard engine. *arXiv preprint arXiv:1308.1525*, 2013.

[32] Christopher Chudzicki, Olufolajimi Oke, and William K Wootters. Entanglement and composite bosons. *Physical review letters*, 104(7):070402, 2010.

[33] Rudi Cilibrasi and Paul MB Vitányi. Clustering by compression. *Information Theory, IEEE Transactions on*, 51(4):1523–1545, 2005.

[34] Richard Cleve and David P. DiVincenzo. Schumacher's quantum data compression as a quantum computation. *Phys. Rev. A*, 54:2636–2650, Oct 1996.

[35] P. T. Cochrane, G. J. Milburn, and W. J. Munro. Macroscopically distinct quantum-superposition states as a bosonic code for amplitude damping. *Phys. Rev. A*, 59:2631–2634, Apr 1999.

[36] M Combescot, F Dubin, and MA Dupertuis. Role of fermion exchanges in statistical signatures of composite bosons. *Physical Review A*, 80(1):013612, 2009.

[37] M Combescot and DW Snoke. Stability of a bose-einstein condensate revisited for composite bosons. *Physical Review B*, 78(14):144303, 2008.

[38] Monique Combescot. "commutator formalism" for pairs correlated through schmidt decomposition as used in quantum information. *EPL (Europhysics Letters)*, 96(6):60002–60007, 2011.

[39] Monique Combescot, Odile Betbeder-Matibet, and François Dubin. The many-body physics of composite bosons. *Physics Reports*, 463(5):215–320, 2008.

[40] Monique Combescot, Shiue-Yuan Shiau, and Yia-Chung Chang. Finite temperature formalism for composite quantum particles. *Physical review letters*, 106(20):206403, 2011.

[41] C. Comte and P. Nozieres. Exciton bose condensation: the ground state of an electron-hole gas-i. mean field description of a simplified model. *Journal de Physique*, 43(7):1069–1081, 1982.

[42] Thomas M. Cover and Joy A. Thomas. *Elements of information theory*. John Wiley & Sons, 2012.

[43] Oscar C. O. Dahlsten, Renato Renner, Elisabeth Rieper, and Vlatko Vedral. Inadequacy of von neumann entropy for characterizing extractable work. *New Journal of Physics*, 13(5):053015, 2011.

[44] Kendall B Davis, M. O. Mewes, M. R. van Andrews, N. J. Van Druten, D. S. Durfee, D. M. Kurn, and Wolfgang Ketterle. Bose-Einstein condensation in a gas of sodium atoms. *Physical Review Letters*, 75(22):3969, 1995.

[45] Francesco De Martini, Valentina Mussi, and Fabio Bovino. Schroedinger cat states and optimum universal quantum cloning by entangled parametric amplification. *Optics communications*, 179(1):581–589, 2000.

[46] Francesco De Martini and Fabio Sciarrino. Colloquium: Multiparticle quantum superpositions and the quantum-to-classical transition. *Reviews of Modern Physics*, 84(4):1765, 2012.

[47] Francesco De Martini, Fabio Sciarrino, and Chiara Vitelli. Entanglement test on a microscopic-macroscopic system. *Physical Review Letters*, 100(25):253601, 2008.

[48] D. Dieks. Communication by EPR devices. *Physics Letters A*, 92(6):271–272, 1982.

[49] Wolfgang Dür, Christoph Simon, and J. Ignacio Cirac. Effective size of certain macroscopic quantum superpositions. *Physical review letters*, 89(21):210402, 2002.

[50] Albert Einstein. Zur allgemeinen molekularen theorie der wärme. *Annalen der Physik*, 319(7):354–362, 1904.

[51] H. S. Eisenberg, G. Khoury, G. A. Durkin, C. Simon, and D. Bouwmeester. Quantum entanglement of a large number of photons. *Phys. Rev. Lett.*, 93:193901, Nov 2004.

[52] J. P. Eisenstein and A. H. MacDonald. Bose–einstein condensation of excitons in bilayer electron systems. *Nature*, 432(7018):691–694, 2004.

[53] Yuval Elias, José M Fernandez, Tal Mor, and Yossi Weinstein. Optimal algorithmic cooling of spins. In *Unconventional Computation*, pages 2–26. Springer, 2007.

[54] Yuval Elias, Haggai Gilboa, Tal Mor, and Yossi Weinstein. Heat-bath cooling of spins in two amino acids. *Chemical Physics Letters*, 517(4):126–131, 2011.

[55] Yuval Elias, Tal Mor, and Yossi Weinstein. Semioptimal practicable algorithmic cooling. *Physical Review A*, 83(4):042340, April 2011.

[56] B. M. Escher, R. L. de Matos Filho, and L. Davidovich. General framework for estimating the ultimate precision limit in noisy quantum-enhanced metrology. *Nature Physics*, 7(5):406–411, 2011.

[57] Mark S. Everitt, Martin L. Jones, Benjamin T. H. Varcoe, and Jacob A. Dunningham. Creating and observing n-partite entanglement with atoms. *Journal of Physics B: Atomic, Molecular and Optical Physics*, 44(3):035504, 2011.

[58] Tristan Farrow and Vlatko Vedral. Classification of macroscopic quantum effects. *arXiv preprint arXiv:1406.0659*, 2014.

[59] Jose M Fernandez, Seth Lloyd, Tal Mor, and Vwani Roychowdhury. Algorithmic cooling of spins: A practicable method for increasing polarization. *International Journal of Quantum Information*, 2(04):461–477, 2004.

[60] Arthur Fine. Hidden variables, joint probability, and the bell inequalities. *Physical Review Letters*, 48(5):291, 1982.

[61] Dale G. Fried, Thomas C. Killian, Lorenz Willmann, David Landhuis, Stephen C. Moss, Daniel Kleppner, and Thomas J. Greytak. Bose-Einstein condensation of atomic hydrogen. *Physical Review Letters*, 81(18):3811, 1998.

[62] F. Fröwis and W. Dür. Are cloned quantum states macroscopic? *Physical Review Letters*, 109(17):170401, 2012.

[63] F. Fröwis, N. Sangouard, and N. Gisin. Linking measures for macroscopic quantum states via photon-spin mapping. *arXiv preprint arXiv:1405.0051*, 2014.

[64] Florian Fröwis and Wolfgang Dür. Measures of macroscopicity for quantum spin systems. *New Journal of Physics*, 14(9):093039, 2012.

[65] A. M. Gavrilik and Yu A. Mishchenko. Energy dependence of the entanglement entropy of composite boson (quasiboson) systems. *Journal of Physics A: Mathematical and Theoretical*, 46(14):145301, 2013.

[66] AM Gavrilik and Yu A Mishchenko. Entanglement in composite bosons realized by deformed oscillators. *Physics Letters A*, 376(19):1596–1600, 2012.

[67] Stefan Gerlich, Sandra Eibenberger, Mathias Tomandl, Stefan Nimmrichter, Klaus Hornberger, Paul J Fagan, Jens Tüxen, Marcel Mayor, and Markus Arndt. Quantum interference of large organic molecules. *Nature Communications*, 2:263, 2011.

[68] R. Ghobadi, S. Kumar, B. Pepper, D. Bouwmeester, A. I. Lvovsky, and C. Simon. Optomechanical micro-macro entanglement. *Physical Review Letters*, 112(8):080503, 2014.

[69] Roohollah Ghobadi, Alexander Lvovsky, and Christoph Simon. Creating and detecting micro-macro photon-number entanglement by amplifying and deamplifying a single-photon entangled state. *Physical Review Letters*, 110(17):170406, 2013.

[70] Roohollah Ghobadi, Sadegh Raeisi, and Christoph Simon. Demonstrating macroscopic entanglement based on Kerr non-linearities requires extreme phase resolution. *arXiv preprint arXiv:1206.3673*, 2012.

[71] Vittorio Giovannetti, Seth Lloyd, and Lorenzo Maccone. Quantum-enhanced measurements: beating the standard quantum limit. *Science*, 306(5700):1330–1336, 2004.

[72] Nicolas Gisin and Serge Massar. Optimal quantum cloning machines. *Physical Review Letters*, 79(11):2153, 1997.

[73] Gilad Gour, Markus P Müller, Varun Narasimhachar, Robert W Spekkens, and Nicole Yunger Halpern. The resource theory of informational nonequilibrium in thermodynamics. *arXiv preprint arXiv:1309.6586*, 2013.

[74] D. M. Greenberger, M. Horne, and A. Zeilinger. Bell's theorem, quantum theory, and conceptions of the universe, 1989.

[75] Allan Griffin, David W Snoke, and Sandro Stringari. *Bose-Einstein Condensation*. Cambridge University Press, 1996.

[76] T. J. Haigh, A. J. Ferris, and M. K. Olsen. Demonstrating mesoscopic superpositions in double-well bose–einstein condensates. *Optics Communications*, 283(18):3540–3547, 2010.

[77] J. Hald, J. L. Sørensen, Christian Schori, and E. S. Polzik. Spin squeezed atoms: a macroscopic entangled ensemble created by light. *Physical Review Letters*, 83(7):1319, 1999.

[78] Dennis A. Hall, Douglas C. Maus, Gary J. Gerfen, Souheil J. Inati, Lino R. Becerra, Frederick W. Dahlquist, and Robert G. Griffin. Polarization-enhanced NMR spectroscopy of biomolecules in frozen solution. *Science*, 276(5314):930–932, May 1997.

[79] David W. Hallwood, Thomas Ernst, and Joachim Brand. Robust mesoscopic superposition of strongly correlated ultracold atoms. *Physical Review A*, 82(6):063623, 2010.

[80] Serge Haroche and Jean-Michel Raimond. *Exploring the quantum: atoms, cavities, and photons (oxford graduate texts)*. Oxford University Press, USA, 2013.

[81] Nick Herbert. Flash-a superluminal communicator based upon a new kind of quantum measurement. *Foundations of Physics*, 12(12):1171–1179, 1982.

[82] Michał Horodecki, Paweł Horodecki, and Jonathan Oppenheim. Reversible transformations from pure to mixed states and the unique measure of information. *Phys. Rev. A*, 67:062104, Jun 2003.

[83] Michał Horodecki and Jonathan Oppenheim. Fundamental limitations for quantum and nanoscale thermodynamics. *Nature Communications*, 4, 2013.

[84] R. S. Ingarden and Kazimierz Urbanik. Information without probability. In *Colloquium Mathematicae*, volume 9, pages 131–150. Institute of Mathematics Polish Academy of Sciences, 1962.

[85] H. Jeong and M. S. Kim. Efficient quantum computation using coherent states. *Physical Review A*, 65(4):042305, 2002.

[86] Hyunseok Jeong, Minsu Kang, and Hyukjoon Kwon. Characterizations and quantifications of macroscopic quantumness and its implementations using optical fields. *Optics Communications*, 2014.

[87] Hyunseok Jeong, Mauro Paternostro, and Timothy C. Ralph. Failure of local realism revealed by extremely-coarse-grained measurements. *Physical Review Letters*, 102(6):060403, 2009.

[88] Jacek Kasprzak, M. Richard, S. Kundermann, A. Baas, P. Jeambrun, J. M. J. Keeling, F. M. Marchetti, M. H. Szymańska, R. Andre, J. L. Staehli, et al. Bose–einstein condensation of exciton polaritons. *Nature*, 443(7110):409–414, 2006.

[89] Phillip Kaye. Cooling algorithms based on the 3-bit majority. *Quantum Information Processing*, 6(4):295–322, 2007.

[90] Wolfgang Ketterle and N. J. Van Druten. Bose-Einstein condensation of a finite number of particles trapped in one or three dimensions. *Physical Review A*, 54(1):656, 1996.

[91] Gerhard Kirchmair, Brian Vlastakis, Zaki Leghtas, Simon E. Nigg, Hanhee Paik, Eran Ginossar, Mazyar Mirrahimi, Luigi Frunzio, S. M. Girvin, and R. J. Schoelkopf. Observation of quantum state collapse and revival due to the single-photon Kerr effect. *Nature*, 495(7440):205–209, 2013.

[92] M. Kitagawa and Y. Yamamoto. Number-phase minimum-uncertainty state with reduced number uncertainty in a Kerr nonlinear interferometer. *Phys. Rev. A*, 34:3974–3988, Nov 1986.

[93] Jan Klaers, Julian Schmitt, Frank Vewinger, and Martin Weitz. Bose-Einstein condensation of photons in an optical microcavity. *Nature*, 468(7323):545–548, 2010.

[94] Johannes Kofler and Časlav Brukner. Classical world arising out of quantum physics under the restriction of coarse-grained measurements. *Physical Review Letters*, 99(18):180403, 2007.

[95] Johannes Kofler and Časlav Brukner. Conditions for quantum violation of macroscopic realism. *Physical Review Letters*, 101(9):090403, 2008.

[96] J. I. Korsbakken, F. K. Wilhelm, and K. B. Whaley. The size of macroscopic superposition states in flux qubits. *EPL (Europhysics Letters)*, 89(3):30003, 2010.

[97] Jan Ivar Korsbakken, K Birgitta Whaley, Jonathan Dubois, and J. Ignacio Cirac. Measurement-based measure of the size of macroscopic quantum superpositions. *Physical Review A*, 75(4):042106, 2007.

[98] Ronnie Kosloff, Eitan Geva, and Jeffrey M. Gordon. Quantum refrigerators in quest of the absolute zero. *Journal of Applied Physics*, 87(11):8093–8097, 2000.

[99] John Kurhanewicz, Daniel B. Vigneron, Kevin Brindle, Eduard Y. Chekmenev, Arnaud Comment, Charles H Cunningham, Ralph J DeBerardinis, Gary G Green, Martin O Leach, Sunder S Rajan, et al. Analysis of cancer metabolism by imaging hyperpolarized nuclei: prospects for translation to clinical research. *Neoplasia*, 13(2):81–97, 2011.

[100] Paweł Kurzyński and Dagomir Kaszlikowski. Information-theoretic metric as a tool to investigate nonclassical correlations. *Physical Review A*, 89(1):012103, 2014.

[101] Pawel Kurzynski, Marcin Markiewicz, and Dagomir Kaszlikowski. On compression of non-classically correlated bit strings. *arXiv preprint arXiv:1310.5644*, 2013.

[102] Paweł Kurzyński, Ravishankar Ramanathan, Akihito Soeda, Tan Kok Chuan, and Dagomir Kaszlikowski. Particle addition and subtraction channels and the behavior of composite particles. *New Journal of Physics*, 14(9):093047, 2012.

[103] Amine Laghaout, Jonas S Neergaard-Nielsen, and Ulrik L. Andersen. Assessments of macroscopicity for quantum optical states. *arXiv preprint arXiv:1405.5062*, 2014.

[104] Antıa Lamas-Linares, Christoph Simon, John C. Howell, and Dik Bouwmeester. Experimental quantum cloning of single photons. *Science*, 296(5568):712–714, 2002.

[105] C. K. Law. Quantum entanglement as an interpretation of bosonic character in composite two-particle systems. *Physical Review A*, 71(3):034306, 2005.

[106] Chang-Woo Lee and Hyunseok Jeong. Quantification of macroscopic quantum superpositions within phase space. *Physical Review Letters*, 106(22):220401, 2011.

[107] K. C. Lee, M. R. Sprague, B. J. Sussman, J. Nunn, N. K. Langford, X-M. Jin, T. Champion, P. Michelberger, K. F. Reim, D. England, et al. Entangling macroscopic diamonds at room temperature. *Science*, 334(6060):1253–1256, 2011.

[108] S.-Y. Lee, J. Thompson, S. Raeisi, P. Kurzynski, and D. Kaszlikowski. Quantum information approach to Bose-Einstein condensate of composite bosons. *ArXiv e-prints*, September 2014.

[109] Su-Yong Lee, Jayne Thompson, Paweł Kurzyński, Akihito Soeda, and Dagomir Kaszlikowski. Coherent states of composite bosons. *Physical Review A*, 88(6):063602, 2013.

[110] Anthony J. Leggett. Testing the limits of quantum mechanics: motivation, state of play, prospects. *Journal of Physics: Condensed Matter*, 14(15):R415, 2002.

[111] Amikam Levy, Robert Alicki, and Ronnie Kosloff. Quantum refrigerators and the third law of thermodynamics. *Physical Review E*, 85(6):061126, 2012.

[112] Adriana E. Lita, Aaron J. Miller, and Sae Woo Nam. Counting near-infrared single-photons with 95% efficiency. *Optics Express*, 16(5):3032–3040, 2008.

[113] Rodney Loudon. *The quantum theory of light*. Oxford university press, 2000.

[114] A. I. Lvovsky, R. Ghobadi, A. Chandra, A. S. Prasad, and C. Simon. Observation of micro-macro entanglement of light. *Nature Physics*, 9(9):541–544, 2013.

[115] Matteo Mariantoni, H. Wang, T. Yamamoto, M. Neeley, Radoslaw C. Bialczak, Y. Chen, M. Lenander, Erik Lucero, A. D. O'connell, D. Sank, et al. Implementing the quantum von neumann architecture with superconducting circuits. *Science*, 334(6052):61–65, 2011.

[116] Florian Marquardt, Benjamin Abel, and Jan von Delft. Measuring the size of a quantum superposition of many-body states. *Physical Review A*, 78(1):012109, 2008.

[117] Lluis Masanes and Jonathan Oppenheim. A derivation (and quantification) of the third law of thermodynamics. *arXiv preprint arXiv:1412.3828*, 2014.

[118] N. David Mermin. Quantum mechanics vs local realism near the classical limit: A bell inequality for spin s. *Physical Review D*, 22(2):356, 1980.

[119] N. David Mermin. Extreme quantum entanglement in a superposition of macroscopically distinct states. *Physical Review Letters*, 65(15):1838, 1990.

[120] C. Monroe, D. M. Meekhof, B. E. King, and D. J. Wineland. A " schrödinger cat" superposition state of an atom. *Science*, 272(5265):1131–1136, 1996.

[121] Tomoyuki Morimae. Necessity of macroscopic operation for the creation of superpositions of macroscopically distinct states. *Physical Review A*, 80(1):012105, 2009.

[122] Tomoyuki Morimae. Superposition of macroscopically distinct states means large multipartite entanglement. *Physical Review A*, 81(1):010101, 2010.

[123] Peter J. Mosley, Jeff S. Lundeen, Brian J. Smith, Piotr Wasylczyk, Alfred B. U'Ren, Christine Silberhorn, and Ian A. Walmsley. Heralded generation of ultrafast single photons in pure quantum states. *Phys. Rev. Lett.*, 100:133601, Apr 2008.

[124] W. J. Mullin. Bose-Einstein condensation in a harmonic potential. *Journal of low temperature physics*, 106(5-6):615–641, 1997.

[125] W. J. Munro, G. J. Milburn, and B. C. Sanders. Entangled coherent-state qubits in an ion trap. *Phys. Rev. A*, 62:052108, Oct 2000.

[126] Eleonora Nagali, Tiziano De Angelis, Fabio Sciarrino, and Francesco De Martini. Experimental realization of macroscopic coherence by phase-covariant cloning of a single photon. *Physical Review A*, 76(4):042126, 2007.

[127] Sarah J. Nelson, John Kurhanewicz, Daniel B. Vigneron, Peder E. Z. Larson, Andrea L. Harzstark, Marcus Ferrone, Mark van Criekinge, Jose W. Chang, Robert Bok, Ilwoo Park, et al. Metabolic imaging of patients with prostate cancer using hyperpolarized [1-13c] pyruvate. *Science translational medicine*, 5(198):198ra108–198ra108, 2013.

[128] Stefan Nimmrichter and Klaus Hornberger. Macroscopicity of mechanical quantum superposition states. *Physical review letters*, 110(16):160403, 2013.

[129] Michael W. Noel and C. R. Stroud Jr. Excitation of an atomic electron to a coherent superposition of macroscopically distinct states. *Physical Review Letters*, 77(10):1913, 1996.

[130] José P. Palao, Ronnie Kosloff, and Jeffrey M. Gordon. Quantum thermodynamic cooling cycle. *Physical Review E*, 64(5):056130, 2001.

[131] James Pawley. *Handbook of biological confocal microscopy*. Springer, New York, 2006.

[132] A. Peres. *Quantum Theory: Concepts and Methods*. Kluwer, 2006.

[133] Christopher Pethick and Henrik Smith. *Bose-Einstein condensation in dilute gases*. Cambridge university press, 2002.

[134] David Pines and Philippe Nozières. *The theory of quantum liquids*. Addison-Wesley, 1990.

[135] TB Pittman, BC Jacobs, and JD Franson. Heralding single photons from pulsed parametric down-conversion. *Optics Communications*, 246(4):545–550, 2005.

[136] S. Portolan, O. Di Stefano, S. Savasta, Fausto Rossi, and R. Girlanda. Decoherence-free emergence of macroscopic local realism for entangled photons in a cavity. *Physical Review A*, 73(2):020101, 2006.

[137] Sadegh Raeisi, Pawel Kurzynski, and Dagomir Kaszlikowski. Entropic version of the Greenberger-Horne-Zeilinger paradox. *arXiv preprint arXiv:1409.7290*, 2014.

[138] Sadegh Raeisi and Michele Mosca. The asymptotic cooling of heat-bath algorithmic cooling. *arXiv preprint arXiv:1407.3232*, 2014.

[139] Sadegh Raeisi, Pavel Sekatski, and Christoph Simon. Coarse graining makes it hard to see micro-macro entanglement. *Physical Review Letters*, 107(25):250401, 2011.

[140] Sadegh Raeisi, Wolfgang Tittel, and Christoph Simon. Proposal for inverting the quantum cloning of photons. *Physical Review Letters*, 108(12):120404, 2012.

[141] Ravishankar Ramanathan, Pawel Kurzynski, Tan Kok Chuan, Marcelo F Santos, and Dagomir Kaszlikowski. Criteria for two distinguishable fermions to form a boson. *Physical Review A*, 84(3):034304, 2011.

[142] Florian Rempp. *Algorithmic cooling and quantumthermodynamic machines*. PhD thesis, Master's thesis, Universitat Stuttgart, 2007.

[143] Florian Rempp, Mathias Michel, and Günter Mahler. Cyclic cooling algorithm. *Physical Review A*, 76(3):032325, 2007.

[144] Max F. Riedel, Pascal Böhi, Yun Li, Theodor W. Hänsch, Alice Sinatra, and Philipp Treutlein. Atom-chip-based generation of entanglement for quantum metrology. *Nature*, 464(7292):1170–1173, 2010.

[145] N. A. Rodriguez Briones and R. Laflamme. Heat-bath algorithmic cooling. In *Poster presented at the Institute for Quantum Computing Scientific Advisory Committee poster session*, March March 2014.

[146] Stefan Rombouts, Dimitri Van Neck, Karel Peirs, and Lode Pollet. Maximum occupation number for composite boson states. *Modern Physics Letters A*, 17(29):1899–1907, 2002.

[147] B. D. Ross, P. Bhattacharya, S. Wagner, T. Tran, and N. Sailasuta. Hyperpolarized mr imaging: neurologic applications of hyperpolarized metabolism. *American Journal of Neuroradiology*, 31(1):24–33, 2010.

[148] C. A. Ryan, O. Moussa, J. Baugh, and R. Laflamme. Spin based heat engine: demonstration of multiple rounds of algorithmic cooling. *Physical Review Letters*, 100(14):140501, 2008.

[149] Pedro Sancho. Compositeness effects, pauli's principle and entanglement. *Journal of Physics A: Mathematical and General*, 39(40):12525, 2006.

[150] Barry C. Sanders. Entangled coherent states. *Phys. Rev. A*, 45:6811–6815, May 1992.

[151] Barry C Sanders. Review of entangled coherent states. *Journal of Physics A: Mathematical and Theoretical*, 45(24):244002, 2012.

[152] Valerio Scarani, Sofyan Iblisdir, Nicolas Gisin, and Antonio Acin. Quantum cloning. *Reviews of Modern Physics*, 77(4):1225, 2005.

[153] Leonard J. Schulman, Tal Mor, and Yossi Weinstein. Physical limits of heat-bath algorithmic cooling. *Physical Review Letters*, 94(12):120501, April 2005.

[154] Leonard J. Schulman, Tal Mor, and Yossi Weinstein. Physical limits of heat-bath algorithmic cooling. *SIAM Journal on Computing*, 36(6):1729–1747, 2007.

[155] Leonard J. Schulman and Umesh Vazirani. Scalable NMR quantum computation. *arXiv:quant-ph/9804060*, April 1998.

[156] BW Schumacher. Information and quantum nonseparability. *Physical Review A*, 44(11):7047, 1991.

[157] Pavel Sekatski, Nicolas Brunner, Cyril Branciard, Nicolas Gisin, and Christoph Simon. Towards quantum experiments with human eyes as detectors based on cloning via stimulated emission. *Physical Review Letters*, 103(11):113601, 2009.

[158] Pavel Sekatski, Nicolas Gisin, and Nicolas Sangouard. How difficult is it to prove the quantumness of macroscropic states? *Phys. Rev. Lett.*, 113:090403, Aug 2014.

[159] Pavel Sekatski, Nicolas Sangouard, and Nicolas Gisin. Size of quantum superpositions as measured with classical detectors. *Physical Review A*, 89(1):012116, 2014.

[160] Pavel Sekatski, Nicolas Sangouard, Magdalena Stobińska, Félix Bussieres, Mikael Afzelius, and Nicolas Gisin. Proposal for exploring macroscopic entanglement with a single photon and coherent states. *Physical Review A*, 86(6):060301, 2012.

[161] Pavel Sekatski, Bruno Sanguinetti, Enrico Pomarico, Nicolas Gisin, and Christoph Simon. Cloning entangled photons to scales one can see. *Physical Review A*, 82(5):053814, 2010.

[162] Akira Shimizu and Takayuki Miyadera. Stability of quantum states of finite macroscopic systems against classical noises, perturbations from environments, and local measurements. *Physical Review Letters*, 89(27):270403, 2002.

[163] Akira Shimizu and Tomoyuki Morimae. Detection of macroscopic entanglement by correlation of local observables. *Physical Review Letters*, 95(9):090401, 2005.

[164] Christoph Simon and Dik Bouwmeester. Theory of an entanglement laser. *Physical review letters*, 91(5):053601, 2003.

[165] Christoph Simon, Gregor Weihs, and Anton Zeilinger. Optimal quantum cloning via stimulated emission. *Physical review letters*, 84(13):2993, 2000.

[166] Ole Winneche Sørensen. Polarization transfer experiments in high-resolution nmr spectroscopy. *Progress in Nuclear Magnetic Resonance Spectroscopy*, 21(6):503–569, 1989.

[167] Nicolò Spagnolo, Chiara Vitelli, Mauro Paternostro, Francesco De Martini, and Fabio Sciarrino. Hybrid methods for witnessing entanglement in a microscopic-macroscopic system. *Physical Review A*, 84(3):032102, 2011.

[168] Nicolò Spagnolo, Chiara Vitelli, Fabio Sciarrino, and Francesco De Martini. Entanglement criteria for microscopic-macroscopic systems. *Physical Review A*, 82(5):052101, 2010.

[169] Hiroyasu Tajima and Masahito Hayashi. Refined carnot's theorem; asymptotics of thermodynamics with finite-size heat baths. *arXiv:1405.6457 [cond-mat, physics:quant-ph]*, May 2014. arXiv: 1405.6457.

[170] A Thilagam. Crossover from bosonic to fermionic features in composite boson systems. *Journal of Mathematical Chemistry*, 51(7):1897–1913, 2013.

[171] Nicholas Thomas-Peter, Brian J. Smith, Animesh Datta, Lijian Zhang, Uwe Dorner, and Ian A. Walmsley. Real-world quantum sensors: Evaluating resources for precision measurement. *Phys. Rev. Lett.*, 107:113603, Sep 2011.

[172] Malte C. Tichy, P. Alexander Bouvrie, and Klaus Mølmer. How bosonic is a pair of fermions? *Applied Physics B*, pages 1–12, 2013.

[173] Malte C. Tichy, P. Alexander Bouvrie, and Klaus Mølmer. Two-boson composites. *Physical Review A*, 88(6):061602, 2013.

[174] Malte C. Tichy, Peter Alexander Bouvrie, and Klaus Mølmer. Bosonic behavior of entangled fermions. *Physical Review A*, 86(4):042317, 2012.

[175] Malte C. Tichy, Peter Alexander Bouvrie, and Klaus Mølmer. Collective interference of composite two-fermion bosons. *Physical review letters*, 109(26):260403, 2012.

[176] Malte C. Tichy, Florian Mintert, and Andreas Buchleitner. Essential entanglement for atomic and molecular physics. *Journal of Physics B: Atomic, Molecular and Optical Physics*, 44(19):192001, 2011.

[177] Akihisa Ukena and Akira Shimizu. Macroscopic entanglement in quantum computation. *arXiv preprint quant-ph/0505057*, 2005.

[178] Chiara Vitelli, Nicolò Spagnolo, Lorenzo Toffoli, Fabio Sciarrino, and Francesco De Martini. Quantum-to-classical transition via fuzzy measurements on high-gain spontaneous parametric down-conversion. *Phys. Rev. A*, 81:032123, Mar 2010.

[179] Tian Wang, Roohollah Ghobadi, Sadegh Raeisi, and Christoph Simon. Demonstrating macroscopic entanglement based on Kerr non-linearities requires extreme phase resolution. In *Frontiers in Optics*, pages FW1C–4. Optical Society of America, 2013.

[180] Tian Wang, Roohollah Ghobadi, Sadegh Raeisi, and Christoph Simon. Precision requirements for observing macroscopic quantum effects. *Physical Review A*, 88(6):062114, 2013.

[181] Hendrik Weimer, Markus J. Henrich, Florian Rempp, Heiko Schröder, and Günter Mahler. Local effective dynamics of quantum systems: A generalized approach to work and heat. *EPL (Europhysics Letters)*, 83(3):30008, August 2008.

[182] Marcin Wieśniak, Vlatko Vedral, and Časlav Brukner. Magnetic susceptibility as a macroscopic entanglement witness. *New Journal of Physics*, 7(1):258, 2005.

[183] Marcin Wieśniak, Vlatko Vedral, and Časlav Brukner. Heat capacity as an indicator of entanglement. *Physical Review B*, 78(6):064108, 2008.

[184] William K. Wootters and Wojciech H. Zurek. A single quantum cannot be cloned. *Nature*, 299(5886):802–803, 1982.

[185] Feng Wu, Lingen Chen, Shuang Wu, Fengrui Sun, and Chih Wu. Performance of an irreversible quantum carnot engine with spin 12. *The Journal of Chemical Physics*, 124(21):214702, June 2006.

[186] Jin-Shi Xu, Man-Hong Yung, Xiao-Ye Xu, Sergio Boixo, Zheng-Wei Zhou, Chuan-Feng Li, Alán Aspuru-Guzik, and Guang-Can Guo. Demon-like algorithmic quantum cooling and its realization with quantum optics. *Nature Photonics*, 8(2):113–118, February 2014.

[187] Benjamin Yadin and Vlatko Vedral. A new criterion for macroscopic quantum states. *arXiv preprint arXiv:1407.2442*, 2014.

[188] Jun Ye, HJ Kimble, and Hidetoshi Katori. Quantum state engineering and precision metrology using state-insensitive light traps. *science*, 320(5884):1734–1738, 2008.

[189] B Yurke and D Stoler. Generating quantum mechanical superpositions of macroscopically distinguishable states via amplitude dispersion. *Physical Review Letters*, 57(1):13, 1986.

[190] Wojciech H Zurek. Thermodynamic cost of computation, algorithmic complexity and the information metric. *Nature*, 341(6238):119–124, 1989.

[191] Wojciech Hubert Zurek. Sub-Planck structure in phase space and its relevance for quantum decoherence. *Nature*, 412(6848):712–717, 2001.

[192] Wojciech Hubert Zurek. Decoherence, einselection, and the quantum origins of the classical. *Reviews of Modern Physics*, 75(3):715, 2003.